Industrial
Chemistry
& Materials

ROYAL SOCIETY
OF CHEMISTRY

MINI REVIEW

View Article Online
View Journal | View Issue

Cite this: *Ind. Chem. Mater.*, 2026, **4**, 151

Non-noble metal single-atom catalysts: controllable fabrication and electrocatalytic CO_2 reduction activity

Chao Xu, Jinbing Wen, Weikang Yuan and Xuezhi Duan *

Received 1st December 2025,
Accepted 3rd February 2026

DOI: 10.1039/d5im00351b

rsc.li/icm

The electrochemical CO_2 reduction reaction (eCO_2RR) was recognized as a pivotal carbon emission reduction technology, as it can couple with renewable energy to convert CO_2 into high-value-added products. With their ultrahigh atomic utilization efficiency, well-defined active sites, and tunable electronic structures, single-atom catalysts (SACs) have demonstrated remarkable catalytic merits and thus exhibited enormous development potential in this field. This minireview summarizes the latest advances in SACs for eCO_2RR. First, the state-of-the-art characterization techniques for single-atom catalysts were discussed, followed by an elaboration on the influence of different synthetic strategies on their performance. Subsequently, the focus was placed on various non-noble metal SACs, with an analysis of the role of catalytic site structures in optimizing the adsorption/desorption energies of intermediates and suppressing the hydrogen evolution side reaction (HER). Finally, the current challenges and prospects of SACs in eCO_2RR were addressed.

Keywords: CO_2 reduction reaction; Electrocatalysis; Synthetic strategies; Single atom.

1 Introduction

Since the Industrial Revolution, the massive combustion of fossil fuels had led to a steady increase in atmospheric CO_2 concentrations.[1] According to NOAA Global Monitoring Laboratory measurements, the average CO_2 concentration in May 2025 hit a record 430.5 ppm (3.6 ppm higher than the previous year), prompting global efforts in emission reduction. The electrochemical CO_2 reduction reaction (eCO_2RR) has emerged as a promising low-carbon technology, as it can convert CO_2 into high-value-added products using renewable electricity under mild conditions.[2–4]

Given the inherent characteristics of thermodynamic inertness and sluggish kinetics in the eCO_2RR, the development

---

State Key Laboratory of Chemical Engineering and Low-Carbon Technology, School of Chemical Engineering, East China University of Science and Technology, Shanghai 200237, China. E-mail: xzduan@ecust.edu.cn

Chao Xu

Dr. Chao Xu obtained his PhD from East China University of Science and Technology (ECUST) in 2023, after which he pursued postdoctoral research at the same institution. His current research interests focus on the design and synthesis of transition metal electrocatalytic materials and electrocatalytic reaction engineering.

Xuezhi Duan

Prof. Xuezhi Duan obtained his PhD in Chemical Engineering from East China University of Science and Technology (ECUST) in 2012. Following a two-year postdoctoral appointment at the Norwegian University of Science and Technology, he joined the academic staff of ECUST's School of Chemical Engineering. He is a full professor and director of the State Key Laboratory of Chemical Engineering and Low-Carbon Technology. His current research interests include mesokinetics-assisted catalyst design and theoretical calculations.

of high-efficiency electrocatalysts has become crucial for advancing this technology from laboratory research to industrial application. The initial step of the eCO_2RR universally entails the adsorption of CO_2 molecules on the catalyst surface, leading to the formation of the adsorbed $*CO_2$ intermediate. This intermediate was subsequently subjected to hydrogenation, affording the key adsorbed intermediates *COOH or *OCOH. Specifically, the *OCOH intermediate undergoes desorption from the catalyst surface to produce HCOOH, whereas the *COOH intermediate undergoes sequential hydrogenation and dehydration processes to form the adsorbed *CO species. Notably, the *CO intermediate exhibits two distinct reaction pathways: desorption from the catalyst surface results in the formation of gaseous CO, while sustained adsorption enables further hydrogenation to yield C_1 products such as CH_4 and CH_3OH. The formation of C_2 products was key dependent on C–C bond coupling, and three possible pathways have been proposed so far: (1) dimerization of two *CO molecules followed by hydrogenation, (2) hydrogenation of *CO to *COH and subsequent coupling with *CO, and (3) hydrogenation coupling of *CO *via* *CHO and $*CH_2O$ intermediates.

Up to now, various catalysts had been developed for the eCO_2RR, with Ag-based[5,6] and Au-based[7,8] nanoparticle catalysts being the most widely used. However, the practical application of catalysts for the eCO_2RR still faces many key challenges: CO_2 molecules feature high thermodynamic stability and complex reduction pathways, leading to poor product selectivity of the catalysts and hindering the targeted synthesis of high-value-added chemicals; the potential windows of the eCO_2RR and the HER overlap significantly, and H^+ in aqueous systems tends to occupy the active sites of the catalysts, thus significantly suppressing the faradaic efficiency of CO_2 reduction; the bulk metal atoms of traditional nanocatalysts can hardly participate in the catalytic reaction, resulting in low metal utilization efficiency.

Over the previous decade, single-atom catalysts (SACs) had been extensively studied by researchers and employed as high-efficiency electrocatalytic materials for the eCO_2RR.[9,10] Notably, their atomic utilization efficiency approaches 100%.[11,12] This feature maximizes the catalytic potential of metal atoms and significantly cuts the dosage of noble metals or the cost of catalysts. It also enables precise regulation of active site density, which is a key factor for balancing eCO_2RR activity and suppressing the competing HER. Moreover, the active sites of SACs feature uniform and well-defined structures, which is not merely an ideal model for investigating general catalytic mechanisms (*e.g.*, structure–activity relationships), but more critically, provides a controllable platform for stabilizing key eCO_2RR intermediates (*e.g.*, $*COOH^{*-}$, $*CO^{*-}$) and regulating their conversion pathways.[13,14] This structural uniformity ensures consistent adsorption energies of reaction intermediates across all active sites, avoiding erratic intermediate adsorption/desorption that would lead to inferior product selectivity. Furthermore, the electronic structure and coordination environment of SACs' metal centers can be flexibly tailored *via* support modification, heteroatom doping, or coordination number adjustment.[15,16] This tunability allows precise matching with the adsorption–desorption energies of eCO_2RR-specific intermediates, lowers the reaction energy barrier for target product formation, and simultaneously suppresses the HER by weakening proton adsorption. Collectively, these advantages of SACs fully highlight their necessity as a core strategy for designing efficient, stable, and low-cost eCO_2RR catalysts, offering broad prospects for advancing the practical application of the eCO_2RR.

In the preparation of SACs, a high-temperature annealing process was usually involved. During this process, metal atoms were thermodynamically prone to spontaneous aggregation into nanoparticles. Meanwhile, both the loading capacity of single atoms and their uniform distribution on the support surface had a significant impact on the aggregation of single atoms.[17–20] In addition, some single atoms might be encapsulated by the support, making them unable to contact reactants and thus affecting catalytic activity. Therefore, to address the aforementioned issues, researchers had developed various synthesis methods, such as wet chemistry method,[21–23] ball milling,[24–26] pyrolysis,[27–29] and atomic layer deposition (ALD) method.[30–32] In recent years, researchers had developed a series of SACs for the eCO_2RR. Among them, noble metal-based SACs such as Au, Pt, Nb, Ag, and Pd had generally exhibited significant advantages in reaction kinetics and long-term stability.[33–37] To further reduce the cost of catalysts, researchers had also developed various non-noble metal-based SACs, and a variety of non-noble metal SACs including Ni, Co, Fe, and Cu had been reported to possess excellent eCO_2RR activity.[37–42]

Against this background, this review focuses on the research progress of SACs in the eCO_2RR, with economical non-noble metal SACs as the core. It systematically covers their advanced characterization techniques, mainstream synthesis strategies and multi-metal center catalytic systems. By clarifying the intrinsic correlation between catalyst structure and catalytic performance, this review provides comprehensive references for basic research and the rational design of catalysts in this field. In addition to summarizing the key achievements of current SACs in optimizing reaction activity, selectivity and stability, it also prospectively points out future development directions such as large-scale preparation, multi-atom synergistic catalysis and industrial application adaptation, thus offering important academic reference and innovative insights for advancing sustainable CO_2 conversion technologies.

2 Characterization techniques of SACs

Determining the geometric structure and electronic environment of single-atom catalysts (SACs) is crucial for revealing their reaction mechanisms and catalytic performance in catalytic processes. By accurately identifying the active sites and surface active species of SACs, and establishing the structure–performance relationship of the catalysts, we can provide a solid theoretical basis and clear experimental guidance for the design and optimization of catalysts. In addition, characterizing the used catalysts enables us to explore the deactivation causes thoroughly and then ensure their sustainability in practical applications through targeted optimization.

2.1 AC-HAADF-STEM

After the preparation of SACs, the primary step was to directly observe the catalysts' micromorphology, structural characteristics, and the single-atom distribution of metal elements by means of material morphology visualization techniques. Compared with conventional technologies such as transmission electron microscopy (TEM) and high-resolution transmission electron microscopy (HRTEM), AC-HAADF-STEM offers superior imaging quality. It enables the accurate identification of the catalysts' fine structures, thereby providing crucial support for revealing their atomic structures and electronic states. This technique's superiority lies in its distinctive imaging mechanism: metal atomic nuclei and incident electron beams exhibit a more intense electrostatic interaction. Metal atoms with higher atomic numbers scatter more electrons at higher angles, thus exhibiting higher contrast than the support matrix in imaging. Du *et al.*[43] prepared an atomically dispersed dual-atom catalyst (InCe/CN) with In and Ce for the eCO_2RR to HCOOH *via* a freeze-drying and annealing method. Using AC-HAADF-STEM, they directly observed numerous isolated bright dots in the InCe/CN catalyst, with no obvious aggregation of metal nanoparticles or clusters. This intuitively confirmed that both In and Ce elements were highly dispersed in the carbon matrix in the form of single atoms. Combined with elemental mapping results, it was further verified that In, Ce, and N elements were uniformly distributed in the catalyst, providing a structural basis for the synergistic effect of the dual-atom sites.

2.2 XAS

Deciphering the valence states and coordination environments of metal atoms in SACs was a core prerequisite for revealing their catalytic activity, selectivity, and reaction mechanisms. This information not only enables precise identification of the chemical nature of active sites and clarification of metal–ligand interactions but also provides key clues for deducing reaction pathways. As an irreplaceable tool for characterizing the metal active sites of SACs, X-ray absorption spectroscopy (XAS) achieves comprehensive analysis of single-atom properties through its core techniques: X-ray absorption near-edge structure (XANES) and extended X-ray absorption fine structure (EXAFS). XANES was highly sensitive to the average valence states and electronic configurations of metal atoms; it can determine the oxidation state *via* the position of the near-edge absorption peak and reveal the electron transfer process between metals and supports. In contrast, EXAFS can obtain core structural parameters such as bond lengths and coordination numbers through data fitting, clarifying the exact positions, arrangement modes, and bonding configurations of metal atoms. These two techniques work synergistically, providing solid experimental support for in-depth interpretation of the catalytic functions of SACs. Chen *et al.*[44] successfully prepared Co–N–C SACs with coordination configurations of $Co–N_3$ and $Co–N_4$ by regulating the order of adding metal precursors, aiming to investigate the influence of the coordination environment on the performance of the eCO_2RR for CO production. XANES analysis revealed that the Co atom in $Co–N_3$ exhibits a lower absorption edge energy, indicating a lower oxidation state compared to that in $Co–N_4$. No Co–Co scattering peak was observed in the EXAFS spectra, confirming that Co atoms were uniformly dispersed in the form of single atoms. Further EXAFS data fitting determined the Co–N coordination numbers of $Co–N_3$ and $Co–N_4$ to be 3.3 and 4.2, respectively, which accurately verified the controllable regulation of the coordination configurations. Combined with electrochemical performance tests and DFT calculations, these XAS characterization results clarified that $Co–N_3$ enhances Co–N interactions and optimizes intermediate adsorption due to its low-coordination and low oxidation state characteristics, thereby exhibiting superior CO_2 reduction activity and selectivity.

2.3 Mössbauer spectroscopy

Mössbauer spectroscopy was based on the phenomenon of recoil-free resonant absorption of γ-rays. By analyzing the variations in the position, shape, and splitting number of characteristic absorption peaks induced by three effects—isomer shift, quadrupole splitting, and magnetic splitting—it can accurately probe the coordination structure and spin state of metal centers in SACs. In Chen *et al.*'s[45] study on the eCO_2RR to HCOOH using single-Cu-atom-modified SnS_2 catalysts (Cu_1/SnS_2), the newly developed rapid freeze-quench (RFQ) ^{119}Sn Mössbauer spectroscopy played a core characterization role. It not only identified the initial state of the catalyst as SnS_2 through *ex situ* measurements but also quantitatively tracked the dynamic evolution of Sn species during the reaction. As the cathodic potential shifts negatively, Cu_1/SnS_2 was gradually reduced to Cu_1/SnS and ultimately converted to Cu_1/Sn. The relative content of metallic Sn increased from 18.3% to 74.2%, which showed a positive correlation with the FE_{COOH} (up to 90.9%) and J_{HCOOH} (158 mA cm^{-2}). Meanwhile, it confirmed that single Cu atoms could accelerate the reduction process of SnS. Combined with the Mössbauer parameters from theoretical calculations, it verified that Cu_1/Sn was the true active site, providing direct experimental evidence for revealing the correlation between catalyst structure evolution and catalytic performance.

3 Synthesis strategies of single-atom catalysts

Since the concept of SACs was proposed in 2011,[46] it had attracted tremendous interest from researchers worldwide due to its exceptional atomic efficiency and its role as an ideal platform for understanding structure–performance relationships. The core logic behind the synthesis of SACs had always centered on two key aspects: "achieving single-atom dispersion" and "stabilizing the existence of single atoms". Therefore, the synthesis of SACs had required attention to several critical parameters: first, breaking the tendency of metal aggregation to prevent metals from attracting each other and agglomerating into nanoparticles; second, possessing sufficient anchoring sites to anchor single atoms on the support through strong interactions, thereby inhibiting migration;[47] third, stabilizing the coordination structure of single atoms to form active centers with both stability and catalytic activity.[48] Based on the above core principles, researchers have developed a series of diverse synthetic methods. By virtue of their precise regulation capabilities over the dispersion state, anchoring effect, and coordination environment of single atoms, these methods can selectively optimize the adsorption–desorption behavior of intermediates in the eCO_2RR, suppress the hydrogen evolution side reaction, and prevent metal agglomeration. They thereby make remarkable contributions to improving the selectivity of target products, increasing the reaction current density, and enhancing the long-term stability of catalysts, providing crucial support for the advancement of the eCO_2RR.

3.1 Wet chemistry method

Wet chemical methods (mainly including co-precipitation and impregnation methods) stand out as a practical and universal strategy for fabricating SACs, benefiting from their simple operation and no requirement for specialized equipment. They can be readily conducted under conventional laboratory conditions, featuring excellent scalability and thus being well-suited for large-scale production demands. The co-precipitation method involved mixing metal salt precursors and support precursors in a liquid phase, forming co-precipitates by adjusting the pH/temperature, and obtaining the product through drying and calcination. The impregnation method utilized a metal precursor solution to impregnate the support, enabling metal species to adhere to the support surface through adsorption/complexation, and the SACs were prepared *via* drying followed by calcination/reduction. This method enables precise regulation of the coordination configuration of single atoms, optimizing the adsorption energies of key intermediates such as *COOH and *CO, thereby enhancing the Faraday efficiency of target products. Li *et al.*[49] had prepared Ln-based SACs with high CO selectivity through the impregnation method. They first obtained C_3N_4 nanosheets by high-temperature pyrolysis of sodium chloride, potassium chloride, and dicyandiamide. Subsequently, they dispersed C_3N_4 carbon nanotubes (CNTs) in deionized water, then added the corresponding metal salt solution. After freeze-drying, pyrolysis was performed to obtain the final catalyst (Fig. 1a). Density functional theory (DFT) calculations had shown that the intermediate *COOH was adsorbed in a bridging mode on Er SACs and in a linear mode on Fe and Ca SACs, while CO was linearly adsorbed on all three SACs (Fig. 1b and c). Charge density difference and Bader charge analyses had indicated that Er SACs exhibited strong adsorption for *COOH (Fig. 1d) and weak adsorption for CO (Fig. 1e). Its unique adsorption mode had circumvented the scaling relationship between *COOH and *CO, facilitating the reduction of CO_2 to CO. Meanwhile, Er SACs also exhibit excellent performance stability. In both

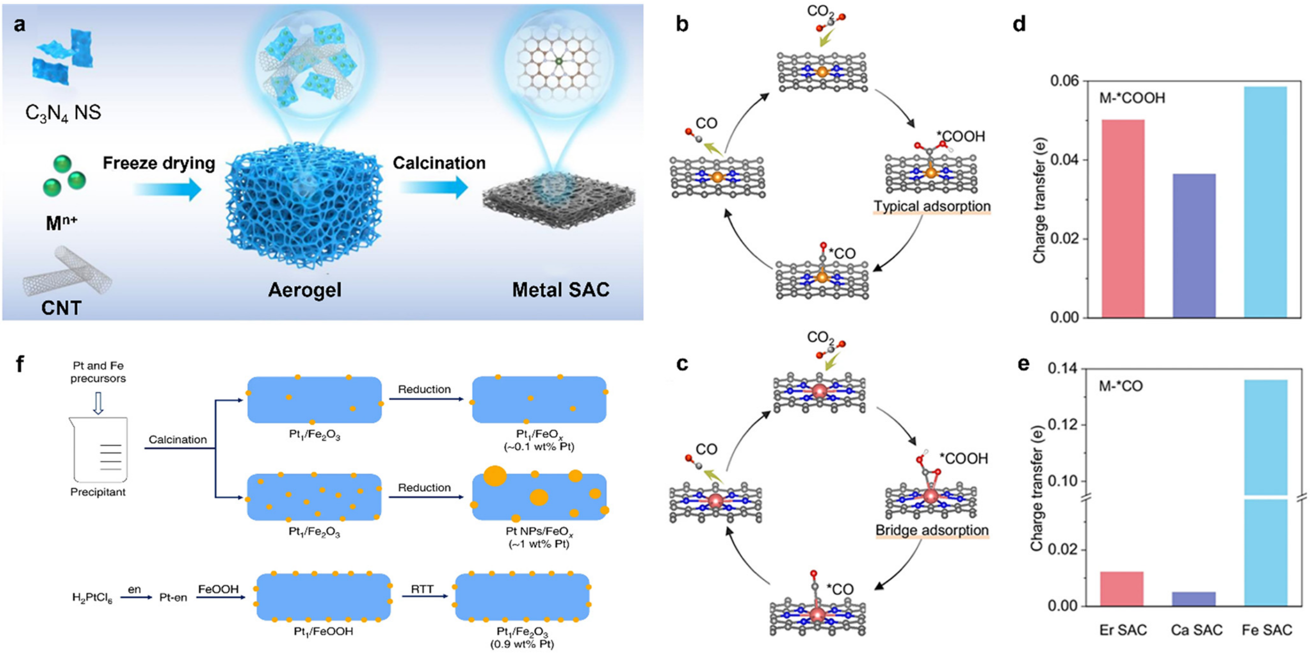

Fig. 1 (a) Schematic illustration of the preparation for metal SAC; structures and adsorption modes of pivotal intermediates adsorbed on Fe SACs (b) and Er SACs (c). Bader charge transfer analysis for the adsorption of *COOH (d) and *CO (e) on SACs. Reprinted with permission from ref. 49. Copyright 2025, Springer Nature. (f) Design concept of the $Pt1/Fe_2O_3$ catalyst. Reprinted with permission from ref. 50. Copyright 2022, Wiley-VCH.

neutral and acidic electrolytes, they can maintain FE_{CO} of over 90% across a wide current density range (50–250 mA cm^{-2}). Specifically, under acidic conditions and a current density of 100 mA cm^{-2}, they can operate stably for 100 hours without significant degradation, and no single-atom agglomeration or support structure collapse is observed after the reaction.

To better achieve atomic-level dispersion of metal precursors during the synthesis process, additives were usually introduced to form complexes with metal precursors, restricting the interactions between metals through the steric hindrance effect. Li *et al.*[50] had used ethylenediamine as a ligand to form a complex with Pt cations. The complex was then fully dispersed and mixed with a pre-prepared suspension of FeOOH support in deionized water. Finally, a single-atom catalyst with a relatively high Pt loading was prepared *via* high-temperature pyrolysis under an inert atmosphere (Fig. 1f).

3.2 Ball milling method

As an important mechanochemical method for preparing single-atom catalysts (SACs), the ball milling method had achieved numerous breakthroughs in recent years prior to that study in aspects such as synthesis strategy innovation, catalytic performance optimization, and mechanism exploration, thanks to its advantages of environmental friendliness and easy scalability. Innovative strategies including top-down grinding, thermally assisted ball milling, and subsurface single-atom preparation had been developed. These strategies could construct abundant defects on the support surface *via* mechanical force, enabling efficient anchoring of various metal single atoms and regulation of their coordination environments through strong metal–support interactions (SMSIs). Metal atoms were firmly anchored through SMSI and even embedded into the subsurface of the support, which effectively inhibits atomic migration and aggregation during electrocatalysis and enhances long-term operational stability. Xia *et al.*[51] prepared an asymmetrically coordinated Ni_1–N_3–S SAC (Ni_1-NSC) *via* ball milling combined with high-temperature calcination. Ball milling enabled thorough mixing of L-cysteine, melamine and nickel nitrate precursors while inducing abundant defects and porous structures in the carbon support to firmly anchor Ni_1–N_3–S active sites. This catalyst exhibited excellent stability in the eCO_2RR: it operated continuously for 210 h at −10 mA cm^{-2} in an H-type cell with negligible changes in FE_{CO} and potential; it underwent stable electrolysis for 10 h at −100 mA cm^{-2} in a flow cell without degradation; and it maintained a CO selectivity of ~94% at −100 mA·cm^{-2} in a membrane electrode assembly (MEA) device.

Dai *et al.*[52] proposed an entropy-driven mechanochemically assisted synthesis strategy for stabilizing Pd single atoms on high-entropy fluorite oxide (HEFO) supports. Specifically, five metal salt precursors (Ce, Zr, Hf, Ti, La), a Pd salt precursor, and fumed silica were first mixed uniformly *via* solvent-free mechanical milling. The mixture was then calcined at 900 °C in an air atmosphere, and a metal oxide composite was formed with the aid of a silica template. During this process, Pd atoms formed stable Pd–O–M bonds (M = Ce/Zr/Hf/Ti/La), with some embedded into the HEFO lattice and others dispersed on the support surface to avoid agglomeration. Finally, the silica template was etched away using NaOH to obtain a porous Pd single-atom catalyst (Fig. 2a). By leveraging the high configurational entropy of HEFO, this strategy reduced the Gibbs free energy through an entropy-driven effect, enabling the stable existence of Pd atoms on the high-entropy support. This addressed the challenge that traditional supports struggle to stabilize single atoms under harsh conditions such as high temperatures. Moreover, the synthesis strategy required no complex regulation, featuring both simplicity and high efficiency.

To address the instability caused by sintering and the poisoning of isolated atoms induced by strong gas adsorption, Guo *et al.*[53] had employed the ball milling method to embed single Cu atoms into the subsurface of Fe_2O_3 supports (Fig. 2b and c). Compared with Cu atoms loaded on the support surface, the Cu atoms embedded in the subsurface had exhibited distinct adsorption properties and reaction mechanisms. Studies had revealed that the subsurface Cu single atoms in Fe_2O_3 could maintain an isolated state under both oxidizing and reducing environments, providing new insights and directions for the design of single-atom catalysts (SACs) with high stability and strong anti-poisoning capability.

3.3 Pyrolysis method

High-temperature pyrolysis had occupied a dominant position in the preparation of single-atom catalysts (SACs) at that time. This method, characterized by mature technology, simple operation, and flexible adaptability to various metals and supports, had been one of the most widely used approaches for synthesizing M–N–C SACs. Furthermore, the strategy of using metal–organic frameworks (MOFs)/covalent organic frameworks (COFs) as precursors or sacrificial templates enables the *in situ* formation of high-density heteroatom anchoring sites, allows precise regulation of the catalyst's active center structure, and facilitates the achievement of high current densities. Lou *et al.*[54] had first prepared sea urchin-like Ni templates *via* a hydrothermal method. Subsequently, they had placed the templates and urea into a ceramic boat and treated the precursor through a two-step annealing process. After mixing with urea, the mixture had undergone two-step annealing under an argon atmosphere. Upon cooling, the product had been soaked in hydrochloric acid to remove nickel cores and unstable substances. After centrifugation, washing, and drying, the sample had been mixed with ammonium chloride and annealed again under an argon atmosphere. The HCl generated from the decomposition of ammonium chloride had etched residual nickel aggregates and allowed nickel ions to be trapped by defects, ultimately yielding atomically dispersed Ni-NC (HPU) SACs (Fig. 3a). The CO_2 reduction activity of the sample had been tested in a hermetically sealed H-type cell with CO_2-saturated 0.5 M $KHCO_3$ solution. The Ni-NC (HPU) catalyst had

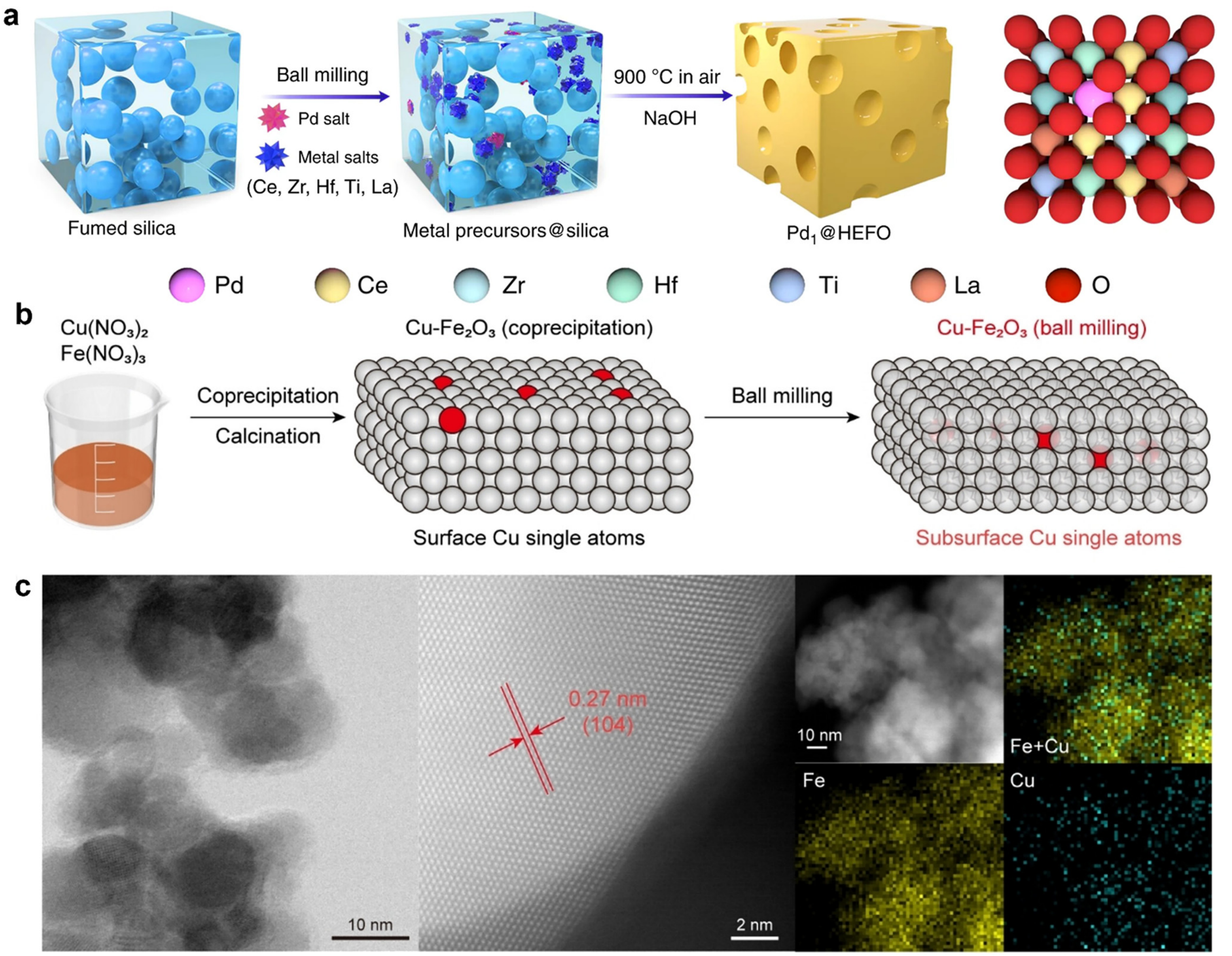

Fig. 2 (a) Synthetic methods of Pd_1@HEFO. Reprinted with permission from ref. 52. Copyright 2024, Springer Nature. (b) Schematic illustration of immersing Cu into Fe_2O_3 *via* ball milling. (c) STEM image and the associated EDS elemental mapping of Fe Kα_1, Cu Kα_1 and Cu + Fe composite. Reprinted with permission from ref. 53. Copyright 2024, Wiley-VCH.

exhibited excellent CO_2 reduction activity, achieving a high selectivity of 91% and a high J_{CO} of 24.7 mA cm^{-2} at −0.8 V *vs.* RHE. Additionally, it showed the lowest Tafel slope, suggesting accelerated kinetics for CO generation (Fig. 3b and d). Meanwhile, the current density of Ni-NC(HPU) remains stable within 30 hours and the FE_{CO} was maintained at around 94% at 0.7 V *vs.* RHE, demonstrating satisfactory stability. Li *et al.*[55] had prepared a two-dimensional (2D) atomically dispersed mesoporous Ni–N–C catalyst *via* a two-step high-temperature pyrolysis process at 500 °C and 800 °C. For the synthesis, thermosetting phenolic resin had been used as the carbon source, dicyandiamide as the nitrogen source, F127 as the structure-directing agent, and nickel nitrate hexahydrate as the metal source, with the addition of acetylacetone and NaCl as the salt template. This catalyst had featured an ultra-thin thickness of 6.7 nm, a high specific surface area of 615 m^2 g^{-1}, and numerous in-plane nanopores. Dicyandiamide had been capable of coordinating with nickel ions and stabilizing nickel single atoms during the carbonization process, achieving high loading density and excellent dispersibility. Furthermore, the 2D ultra-thin mesoporous structure had facilitated gas diffusion and three-phase interface reactions. The catalyst exhibits a CO selectivity exceeding 95% at a high current density of 446 mA cm^{-2} when tested in a flow cell. After loading the catalyst into the MEA, the current density decreases minimally over 50 hours of operation, while the FE_{CO} remains above 90%. Aberration-corrected HAADF-STEM characterization reveals that the 2D ultra-thin mesoporous structure of the catalyst does not undergo significant changes, and the nickel sites remain atomically dispersed without agglomeration.

As a zeolitic imidazolate framework (ZIF)-type MOF material, ZIF-8 had emerged as an excellent template for the preparation of SACs due to its unique spatial confinement structure and thermally decomposable property. The core synthesis strategy had been to encapsulate metal precursors by virtue of the spatial confinement effect of ZIF-8, followed by processes such as pyrolysis to prepare SACs. Jiang *et al.*[56] had dissolved nickel nitrate hexahydrate and zinc nitrate

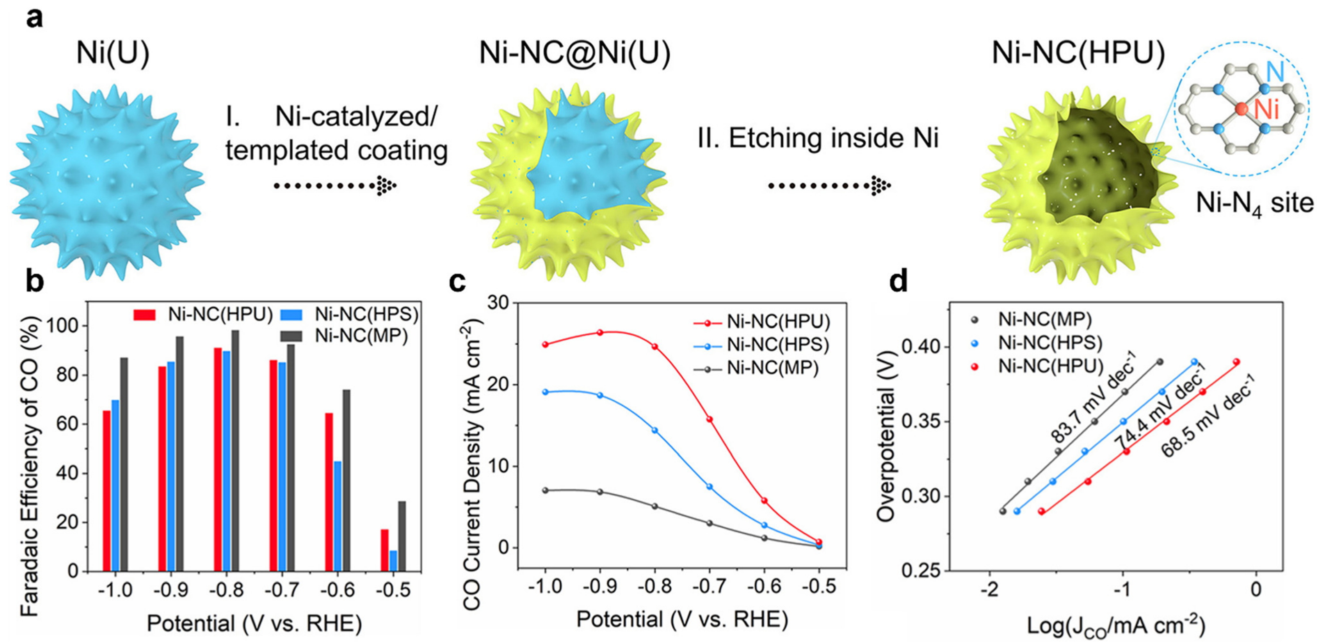

Fig. 3 (a) Schematic illustration of the preparation strategy for Ni-NC(HPU); (b) comparison of CO FE of Ni-NC(HPU), Ni-NC(HPS) and Ni-NC(MP) at various potentials; (c) CO partial current density comparison at a series of potentials; (d) Tafel plots for CO production. Reprinted with permission from ref. 54. Copyright 2024, Wiley-VCH.

hexahydrate in methanol to form solution A, which had been mixed with solution B (2-methylimidazole dissolved in methanol). After stirring at room temperature, the mixture had been washed with ethanol and dried under vacuum to obtain Ni-ZIF-8. Ni-ZIF-8 and KCl had been calcined at high temperature under nitrogen protection to synthesize a Ni–N–C catalyst with abundant defect sites and a mesoporous structure (Fig. 4a). This catalyst had exhibited a high CO

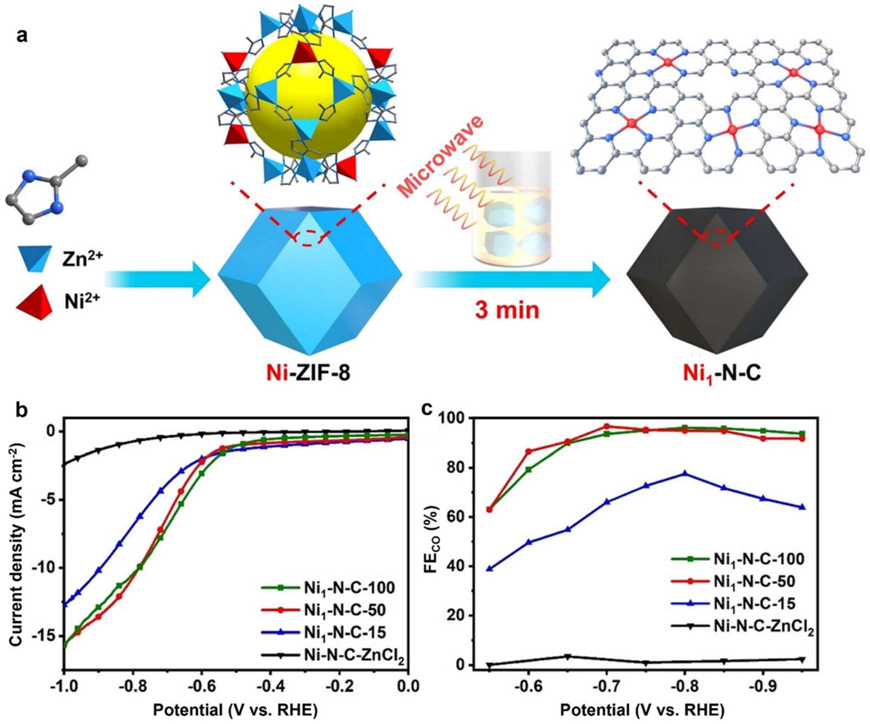

Fig. 4 (a) Schematic diagram of the synthesis method for Ni_1–N–C; (b) LSV curves of various catalysts; (c) FE_{CO} of various catalysts. Reprinted with permission from ref. 56. Copyright 2024, Wiley-VCH.

partial current density (j_{CO} = 1.06 A cm^{-2}) (Fig. 4b) and a CO Faraday efficiency of 96% in the electrochemical CO_2 reduction reaction (Fig. 4c), which had been attributed to the promotion of CO_2 adsorption and mass transfer by the mesoporous and defect structures.

3.4 ALD method

The core principle of preparing SACs *via* ALD had been to leverage its self-limiting surface reaction characteristics. First, the support had been pretreated to activate surface active sites. Subsequently, metal precursors and reactive gases had been alternately pulsed into the reaction chamber: metal precursors had formed a monolayer coverage on the support surface through chemisorption or physisorption, and the subsequently introduced reactive gases had undergone chemical reactions with the adsorbed precursors to anchor metal atoms on the active sites of the support. This strategy enables 100% uniform dispersion of metal atoms with highly tunable coordination environments, which can precisely match the adsorption–desorption energy barriers of reaction intermediates, thereby significantly enhancing the selectivity of target products. However, this method has limitations such as harsh experimental conditions and high equipment costs, restricting its large-scale application. Sun *et al.*[57] proposed a universal method for preparing pyrrolic-N_4 coordinated single-atom catalysts *via* ALD (Fig. 5a). First, Pt single atoms were deposited on the surface of nitrogen-doped carbon nanosheets (NCNS) by ALD to form Pt_1/NCNS. Then, using metallocenes as precursors, Fe, Co, and Ni were loaded onto Pt_1/NCNS *via* ALD under the catalysis of Pt_1 atoms, which promoted the combination of these metals with pyrrolic-N_4 sites. Finally, ligands were removed by introducing O_2, resulting in highly dispersed M_1Pt_1/NCNS catalysts, with Pt remaining atomically dispersed throughout the process. John M. Vohs *et al.*[58] had developed a modified ALD method named diluted atomic layer deposition (DALD) (Fig. 5b). By exposing the sample to the vapor of M(acac)$_x$ precursor solution diluted with acetylacetone (Hacac), the metal deposition rate per ALD cycle had been precisely controlled. By adjusting the ratio of M(acac)$_x$ to Hacac, the metal deposition rate per cycle of Rh, Ir, and Pt on γ-Al_2O_3 had been tuned from approximately 1 metal atom per nm^2 to as low as 0.01 atom nm^{-2}, enabling the controllable deposition from mixtures of nanoparticles, small clusters, and single atoms to pure single atoms (Fig. 5c).

In summary, a variety of synthesis methods had been developed by then to prepare SACs with high dispersibility and stability. Details of the comparative evaluation of various synthesis routes are provided in Table 1. The rational selection of precursors, precise screening and modification of supports, and appropriate adaptation of synthesis methods had all played key roles in achieving the single-atom dispersion of metal atoms. By means of mechanisms such as inhibiting metal aggregation, constructing anchoring sites, and enhancing metal–support interactions (SMSI), the critical bottleneck of atomic migration and aggregation had been broken through, ultimately realizing the atomic-level dispersion and stable existence of metal atoms and providing highly efficient active centers for catalytic reactions.

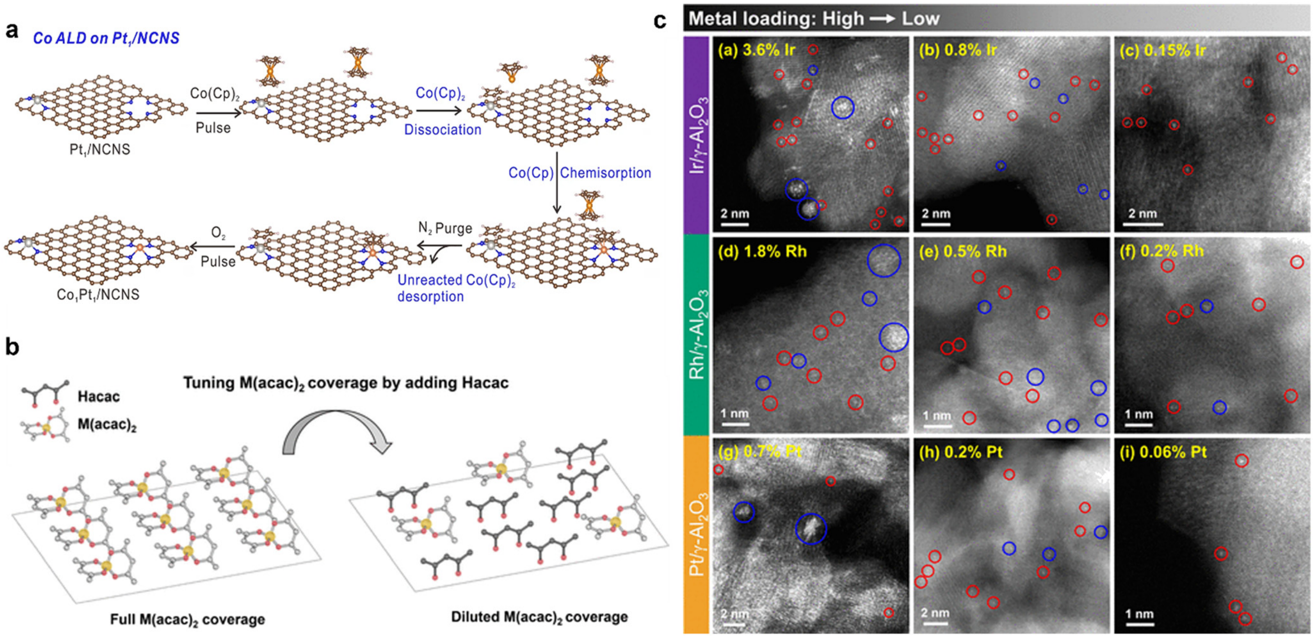

Fig. 5 (a) Schematic diagram of M_1Pt_1/NCNS catalyst synthesis. Reprinted with permission from ref. 57. Copyright 2021, Springer Nature. (b) Schematic diagram comparing the precursor adsorption differences between ALD and DALD. (c) HAADF-STEM images of γ-Al_2O_3-supported catalysts with different metals and varying metal weight loadings. Reprinted with permission from ref. 58. Copyright 2025, American Chemical Society.

Table 1 Synthesis methods and evaluation of SACs

Property	Wet chemistry	Ball milling	Pyrolysis	ALD
Principle	Adsorption, complexation, or co-precipitation of metal salts and support precursors in the liquid phase	Mechanical force creates support defects, and strong metal–support interactions anchor single atoms and regulate the coordination environment	The framework structure serves as a self-template; high-temperature pyrolysis stabilizes single atoms	*Via* self-limiting reaction between precursors and support surface, alternate pulse-deposition of metal atoms and reactive gases
Advantages	Scalable, industrially feasible, straightforward fabrication	Solvent-free, scalable, low-cost	High-loading, porous-tunable, good dispersibility	Atomic precision, controllable dispersion
Disadvantages	Easy agglomeration, solvent residue risk	Dispersion uncontrollability, coordination tunability limitation	Structural collapse risk, inhomogeneous dispersion at high loading	High equipment requirement, limited scalability
Scalability potential	High (operational simplicity)	High (solvent-free, short process)	Medium (high energy consumption at elevated temperatures)	Low (high equipment cost, long cycle)

4 Non-noble metal SACs for the eCO_2RR

With the advancement of global carbon neutrality goals, the eCO_2RR had attracted extensive attention from the scientific community as a key technology for achieving carbon resource recycling and alleviating energy crises and environmental pressures. SACs had emerged as highly efficient candidate catalysts due to their unique advantages such as near-100% atomic utilization efficiency, uniform active sites, and excellent selectivity. By precisely regulating the coordination environment, support interactions, and electronic structure of metal active centers, these catalysts could directionally optimize key steps including CO_2 activation, intermediate adsorption, and product desorption, thereby efficiently realizing the highly selective conversion of target products such as CO, formate, and multi-carbon compounds. Numerous studies had shown that Au-based and Ag-based SACs were efficient and stable eCO_2RR catalysts. Hu *et al.*[86] constructed gold single-atom catalysts (Au_1/hNCNC) on hierarchical nitrogen-doped carbon nanocages (hNCNCs) *via* an impregnation–drying method and applied them for the first time to electrocatalytic CO_2 reduction to syngas. The catalyst exhibited a high mass activity of 3319 A g_{Au}^{-1} at −1.0 V (*vs.* RHE), which was far superior to that of gold nanoparticle catalysts. Moreover, the H_2/CO ratio of the produced syngas could be tuned in the range of 0.4–2.2 by regulating the applied potential. Theoretical studies revealed that this ratio tunability originated from the distinct responses of the HER and the eCO_2RR at the gold single-atom sites coordinated with single nitrogen atoms. The enhanced catalytic activity was associated with the smooth switching between the twofold and the fourfold coordination of gold atoms during the reaction, which reduced the free energy of the rate-determining step. Additionally, the catalyst showed good retention of current density and product selectivity in a 10 hour stability test. Zhuang *et al.*[87] prepared a Ag-SAC with a tri-nitrogen coordination structure anchored on porous concave nitrogen-doped carbon (Ag_1–N_3/PCNC). It achieved a FE_{CO} of up to 95% at −0.37 V *vs.* RHE and a J_{CO} of 7.6 mA cm^{-2} at −0.55 V *vs.* RHE. *In situ* attenuated total reflectance surface-enhanced infrared absorption spectroscopy (ATR-SEIRAS) indicated that the Ag_1–N_3 single-atom sites exhibited weaker adsorption toward the reaction intermediate CO, which facilitated CO desorption and thus enhanced catalytic activity and selectivity. Moreover, the catalyst maintained high current density and product selectivity during a 40 hour stability test. However, the limited reserves and high cost of noble metals have impeded their large-scale practical applications. As an alternative, non-noble metal-based SACs had exhibited remarkable electrocatalytic eCO_2RR performance (Table 2), which had been more in line with the requirements of industrial applications and had held great promise for replacing noble metal catalysts as the mainstream.

4.1 Ni-based SACs

Ni-SACs had been non-noble metal catalysts with great application potential in the eCO_2RR. The valence shell electronic configuration of Ni ($3d^84s^2$) had enabled it to form stable coordination structures such as M–N_4 and M–O_x with supports (*e.g.*, nitrogen-doped carbon, metal oxides, *etc.*).[88] Meanwhile, by adjusting the d-band center position of Ni, a high match could be achieved between their adsorption energies and those of key intermediates in the eCO_2RR, thereby enhancing the selectivity and conversion efficiency of CO. Yu *et al.*[89] had regulated the catalytic activity of Ni-SACs by introducing F atoms into Ni-SAC (Fig. 6a). DFT calculations and experimental characterization had confirmed that F doping could modify the electronic structure of the central Ni–N_4 sites, reduce the energy barrier for CO_2 activation, and promote the formation of the key intermediate *COOH. This catalyst had exhibited excellent CO_2-to-CO conversion performance: the FE_{CO} had exceeded 99% over a wide potential range of −0.7 to −1.0 V *vs.* RHE (Fig. 6b), the turnover frequency (TOF) had reached 9.5×10^4 h^{-1} at −1.16 V, a practical current density of 400 mA cm^{-2} had been achieved in a MEA with CO selectivity maintained above 95%, and it had possessed stable durability for more than 14 hours (Fig. 6c and d).

Table 2 Non-noble metal SACs for the eCO_2RR

Electrocatalyst	Electrolyte	Reactor	Potential (V *vs.* RHE)	FE_{CO}%	j_{CO} (mA cm^{-2})	Ref.
Fe-NS-C	0.1 M $KHCO_3$	H-cell	−0.58	98.0	7.0	59
Fe–N/P–C	0.5 M $KHCO_3$	—	−0.45	98.0	2.0	60
Fe-N-CF	0.5 ml L^{-1} $NaHCO_3$	H-cell	−0.51	97.0	5.4	61
FeNCs-FeSAs/NPC	0.5 M $KHCO_3$	—	−0.70	97.7	8.0	62
SA-Fe/NG-600	0.1 M $KHCO_3$	—	−0.60	98.0	23.7	63
FeN@C-ID	0.5 M $KHCO_3$	H-cell	−0.60	96.9	9.1	64
Fe-SAC/PSNC	1 M KOH	Flow cell	—	98	100	65
FeS@PC	0.5 M $KHCO_3$	H-cell	−0.60	97	5.8	66
Fe_1-NSC	0.5 M $KHCO_3$	—	−0.48	98.6	5.0	67
$Fe–S_1N_3$	0.1 M $KHCO_3$	Flow cell	−0.50	99.2	77.1	68
$Ni–N_2–C$	0.5 M $KHCO_3$	H-cell	−0.8	98.0	10.0	69
Ni-SAC-CNT	1 M KOH	Flow cell	−0.35	99.0	200.0	70
NiSA/NP	0.5 M $KHCO_3$	—	−0.80	99.0	40.0	71
NiSA(0.3)-N-GC	0.1 M $KHCO_3$	H-cell	−0.76	97.2	27.5	72
Ni SAC-1000	0.5 M $KHCO_3$	—	−0.80	98.2	42	73
$Ni–N_2O_2$	0.5 M $KHCO_3$	H-cell	−0.83	97.4	6.5	74
Ni1-NC SAC	0.5 M $KHCO_3$	—	−0.80	90.6	14.6	75
Ni_6@$Ni–N_3$	0.5 M $KHCO_3$	H-cell	−1.0	95.0	43.5	76
NiNC-1100	0.5 M $KHCO_3$	H-cell	−0.66	99.0	10.0	77
L–Ni–NC–C	0.1 M $KHCO_3$	H-cell	−0.70	99.1	7.5	78
CoPc@ZnOv	0.1 M $KHCO_3$	H-cell	−1.0	97.2	—	79
$Co–N_2C_3$	0.1 M $KHCO_3$	—	−0.80	92.0	8.3	80
CoN_4	0.1 M $KHCO_3$	H-cell	−1.1	93.0	12.3	81
CoSAs-Pc	0.1 M $KHCO_3$	H-cell	−0.80	94.8	11.4	82
$Co–N_5$/HNPCSs	0.2 M $NaHCO_3$	—	−0.79	99.4	—	83
$Mn–C_3N_4$/CNT	0.5 M $KHCO_3$	—	−0.55	98.8	14.0	84
$Cu/N_{0.14}C$	0.1 M $KHCO_3$	—	−1.10	51.0 (ethanol)	14.4	85

Shen *et al.*[90] had prepared $Ni–X–N_3–C$ (X: S, Se, Te) SACs with asymmetric coordination structures by introducing chalcogen heteroatoms (S, Se, Te) into the symmetric $Ni–N_4–C$ configuration *via* gas-phase methods. Studies had found that the introduction of heteroatoms had broken the original coordination symmetry and induced charge redistribution, among which $Ni–Se–N_3–C$ had shown the optimal performance: the CO selectivity had been as high as ∼98% at −0.70 V *vs.* RHE, the CO partial current density (j_{CO}) had reached 53.9 mA cm^{-2} at −0.85 V, and it had maintained good stability. *In situ* spectroscopic characterization and DFT calculations had confirmed that the introduction of Se atoms could significantly elevate the d-band center of central Ni atoms, reduce the energy barrier of the rate-determining step (COOH formation), and effectively suppress the HER (Fig. 6e–g). In summary, Ni-based SACs exhibit excellent performance in the electrochemical reduction of CO_2 to CO, benefiting from their optimal *COOH and facile CO desorption properties. Heteroatom doping, which modulates the electronic structure, optimizes the d-band center, or breaks coordination symmetry, and plays a crucial regulatory role in catalytic activity, selectivity, and stability. This work had provided a new idea for the design of eCO_2RR catalysts with high activity and selectivity.

4.2 Fe-based SACs

The valence shell electronic configuration of Fe had endowed it with flexible valence adjustability, enabling it to form moderate electronic interactions with key intermediates of the eCO_2RR (*e.g.*, *COOH, *CO). These interactions had not only ensured the formation of *COOH but also avoided active site blocking caused by excessive product adsorption. Regarding the controversial mechanism underlying the high activity of Fe(III)-NC SACs in the eCO_2RR, Xiao *et al.*[91] had for the first time clarified *via* DFT calculations that the coordination model of Fe(III)-NC was $FeN_1C_3–C$. Studies had revealed that under eCO_2RR operating conditions, Fe(III)–N_1C_3–C would break all Fe–C bonds, forming a novel transient pendant active site—where the Fe single atom was stably bound to the support solely through Fe–N bonds. *Ab initio* molecular dynamics (AIMD) simulations had confirmed the dynamic stability of this $(H_2O)_3–FeN_1(CH)_3–C$ structure in the electrolyte.

Zhang *et al.*[92] successfully constructed a covalent oxygen-bridged single Fe atom catalyst supported on carbon nanotubes (FePc-O-CNT) *via* a covalent oxygen-bridging strategy, which was mainly composed of low-spin (LS) Fe(III) sites. This catalyst had exhibited excellent performance in eCO_2RR: the FE_{CO} had reached 99% at −0.7 V *vs.* RHE, and the turnover frequency (TOF) had reached 5.3×10^4 h^{-1}, more than 20 times higher than that of FePc-CNT containing only high-spin (HS) Fe(III) sites. By means of characterization techniques such as *in situ* and rapid freeze-quench ^{57}Fe Mössbauer spectroscopy (Fig. 7a–d) and *in situ* X-ray absorption spectroscopy (Fig. 7e and f), it had been found that HS Fe(II) sites generated *in situ* under low overpotentials dominated the eCO_2RR, while LS Fe(II) sites were

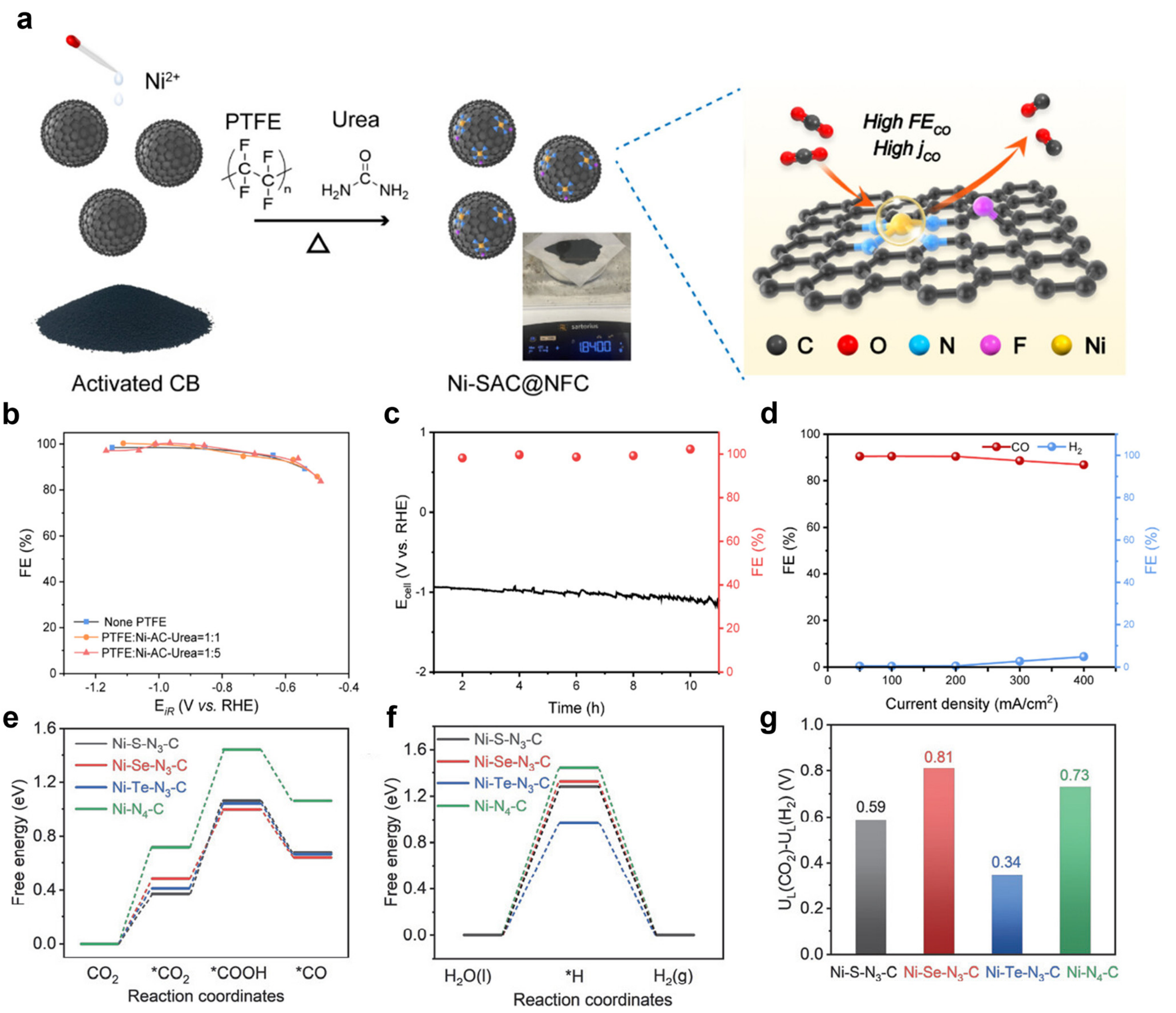

Fig. 6 (a) Schematic diagram of the Ni-SAC@NFC preparation method; (b) FE_{CO} of catalysts with different F contents; (c) stability measurement of Ni-SAC@NFC; (d) FE_{CO} of Ni-SAC@NFC in MEA. Reprinted with permission from ref. 89. Copyright 2024, American Chemical Society. Reaction pathways and free energy diagrams for the eCO_2RR (e) and HER (f) over heteroatom-doped catalysts at 0 V *vs.* RHE; (g) limiting potential differences between the eCO_2RR and the HER for the catalysts. Reprinted with permission from ref. 90. Copyright 2024, Elsevier.

predominant under high overpotentials. *In situ* Raman spectroscopy and ATR-SEIRAS had revealed that the one-electron reduction of the phthalocyanine ring weakened the CO binding strength on LS O–Fe(II)Pc⁻ sites, facilitating CO desorption. DFT calculations had further confirmed that the Bader charge of LS O–Fe(II)Pc⁻ sites increased and the d-band center shifted upward, which reduced the free energy barrier for the formation of the *COOH intermediate and simultaneously suppressed the HER. In conclusion, Fe-based SACs exhibit excellent CO_2-to-CO conversion capability due to the adaptability between their dynamically tunable electronic structures (spin states, oxidation states) and key intermediates (*CO, *COOH). Coordination environment reconstruction and regulation of the d-band center position have demonstrated great advantages in enhancing catalytic activity and CO selectivity. These findings highlight the enormous potential of Fe-based SACs as high-performance catalysts for CO production *via* eCO_2RR.

4.3 Co-based SACs

Co-SACs had been high-performance non-noble metal catalysts in the electrocatalytic eCO_2RR, and the design of the coordination structure of their Co active centers had played a crucial role in their catalytic activity and selectivity.[93] To investigate the influence of the microenvironment of SACs on eCO_2RR, Xiong *et al.*[94] had prepared three cobalt single-atom catalysts with different Co–N_4 microenvironments *via* a pyrolysis strategy using various nitrogen-containing precursors (1,10-phenanthroline, 2-methylimidazole, and 4-dimethylaminopyridine), namely

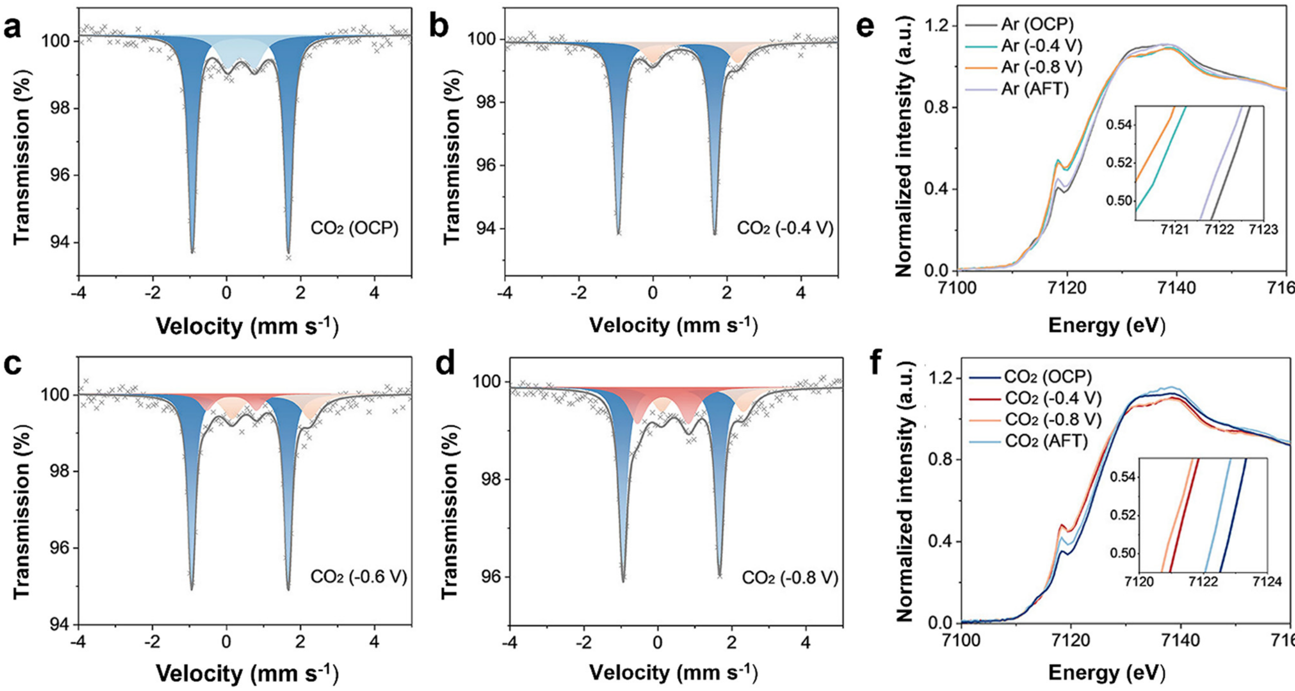

Fig. 7 (a–d) Room-temperature Mössbauer spectra acquired at open-circuit potential (OCP), −0.4, −0.6, and −0.8 V *vs.* RHE in CO_2-saturated 0.5 M $KHCO_3$ electrolyte. (e and f) Fe K-edge XANES of FePc-O-CNT at OCP, −0.4, −0.8 V *vs.* RHE, and after-CO_2RR (AFT) in Ar/CO_2-saturated 0.5 M $KHCO_3$. Reprinted with permission from ref. 92. Copyright 2025, American Chemical Society.

pyridinic Co–N_4 (Co–N_4 SAC_{phen}), pyrrolic Co–N_4 (Co–N_4 SAC_{Dp}), and mixed Co–N_4 (Co–N_4 SAC_{Mm}). Studies had found that the Co–N_4 SAC_{phen} had exhibited the optimal performance: the FE_{CO} had reached as high as 99.5% at −0.76 V *vs.* RHE, and the FE_{CO} had been maintained above 90% over a wide current density range of 50–250 mA cm^{-2} in a flow cell with good stability for 10 hours. In contrast, the pyrrolic Co–N_4 SAC_{Dp} had been prone to the HER, resulting in poor CO selectivity and stability. Experimental characterization had confirmed that pyridinic N had been more conducive to electron accumulation and delocalization, promoting the formation of the *COOH intermediate and reducing the reaction energy barrier. Moreover, the pyridine content had shown a positive correlation with CO selectivity. This study had provided important insights for optimizing eCO_2RR performance by regulating the microenvironment of M–N_4 single-atom catalysts.

The asymmetric coordination structure formed by partially substituting N ligands with heteroatoms (*e.g.*, S, P, O) had been a key strategy to enhance catalytic performance. For example, Zhuang *et al.*[95] had proposed a thermal substitution synthesis strategy. Using Co-ZIF-8 as the precursor and thiobenzene as the sulfur source, they had achieved the gradual substitution of nitrogen atoms with sulfur atoms at the Co–N_4 sites in cobalt single-atom catalysts by adjusting different pyrolysis temperatures, successfully preparing a series of single-atom catalysts with tunable coordination environments (Co–S_xN_{4-x}, x = 0, 1, 2, 3) (Fig. 8a). Studies had revealed a volcano-type relationship between the electrochemical CO_2 reduction performance of these catalysts and their coordination structures. Among them, the Co–S_1N_3 catalyst had exhibited excellent catalytic performance due to the optimal balance between the binding strengths of the key reaction intermediates *COOH and *CO: the CO Faraday efficiency had been as high as ~98% at an overpotential of 410 mV, with a TOF of 4564 h^{-1}; in flow cell tests, it had maintained a CO selectivity above 90% over a wide current density range of 50–225 mA cm^{-2} and had shown good stability after continuous operation for 50 hours. Combined with DFT calculations and experimental characterization, as the number of Co–S coordination increases (x = 0–3), the Bader charge of the Co center decreases continuously from 0.36 e^- for Co–N_4 to −0.25 e^- for Co–S_3N_1, and the adsorption strength of COOH* and CO* intermediates is synchronously enhanced. Among them, the energy barrier for COOH* formation gradually decreases, while the energy barrier for CO* desorption continuously increases. This results in the RDS of Co–N_4 being COOH* formation, while the RDS of Co–S_2N_2 and Co–S_3N_1 shifts to CO* desorption. In contrast, Co–S_1N_3 achieves a balance between the adsorption energies of the two intermediates. The theoretical limiting potentials of the four catalysts were 0.79 eV for Co–N_4, 0.37 eV for Co–S_1N_3, 0.78 eV for Co–S_2N_2, and 0.84 eV for Co–S_3N_1. Co–S_1N_3 exhibits the lowest limiting potential and the most positive limiting potential difference between the eCO_2RR and the HER, corresponding to the optimal catalytic activity and CO selectivity. This thermal substitution strategy had provided a feasible method for precisely regulating the local coordination environment of SACs and had offered important references for the design of high-efficiency eCO_2RR catalysts.

Precise adjustment of the coordination number had been able to optimize the catalytic activity and structural stability of

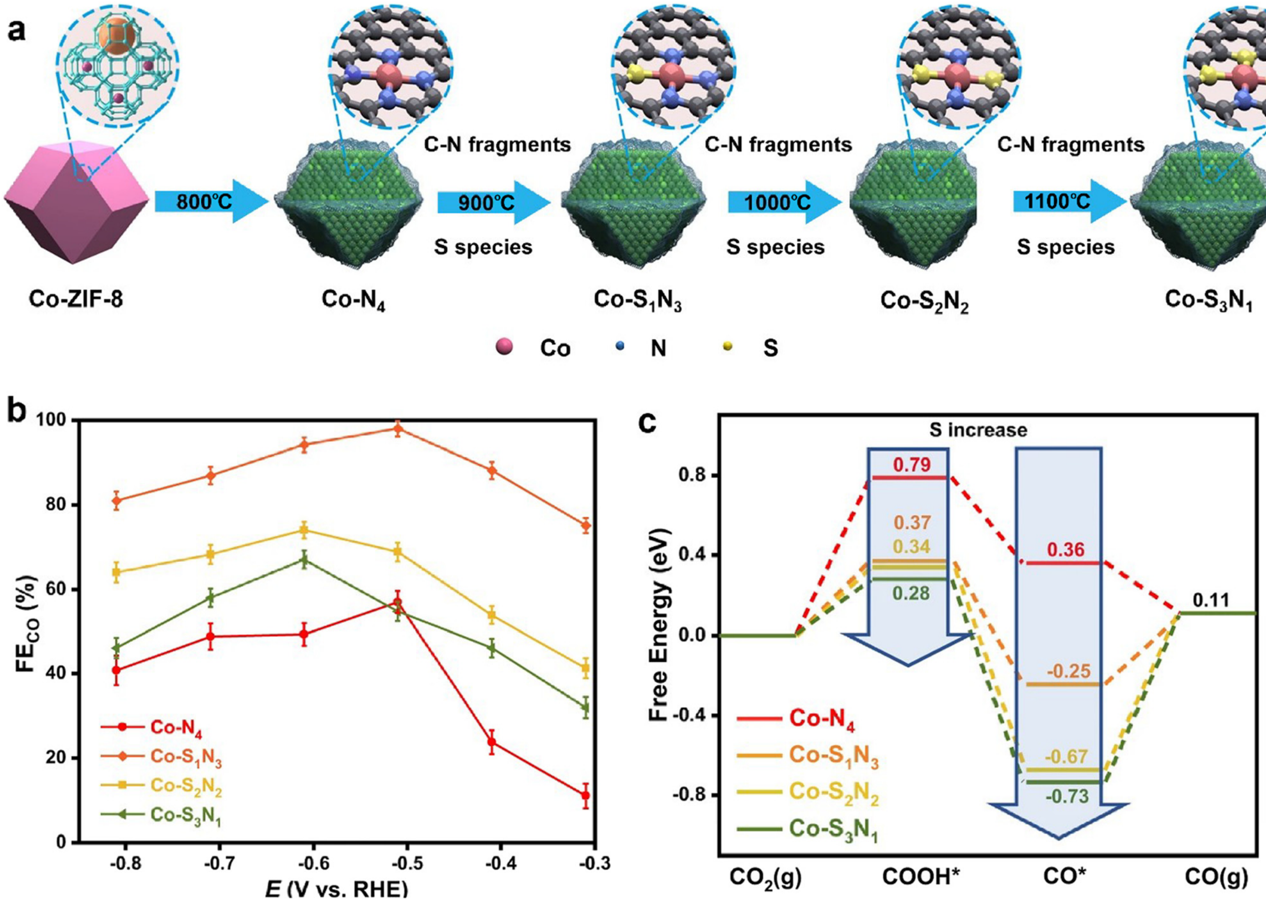

Fig. 8 (a) Schematic illustration of Co–S_xN_{4-x} SACs synthesis; (b) FE_{CO} of the Co–S_xN_{4-x} SACs at different voltages; (c) free energy profiles of CO_2 reduction to CO on Co–S_xN_{4-x} SCs. Reprinted with permission from ref. 95. Copyright 2025, Springer Nature.

Co-SACs. Reducing the coordination number had increased the unsaturation of the Co center and enhanced its ability to activate CO_2. Li *et al.*[96] had used Co/Zn ZIFs as the precursor and controlled the release of volatile CN fragments by adjusting the pyrolysis temperature, successfully preparing a series of atomically dispersed cobalt catalysts with different nitrogen coordination numbers (Co–N_2, Co–N_3, Co–N_4) (Fig. 9a). Studies had found that the coordination environment of cobalt atoms had significantly influenced the eCO_2RR performance, with the Co–N_2 catalyst showing the most excellent performance: at an overpotential of 520 mV, the FE_{CO} had reached 94% (Fig. 9b), the current density had been 18.1 mA cm^{-2}, which was much higher than those of Co–N_3, Co–N_4, and cobalt nanoparticle catalysts. Additionally, it had maintained good stability after continuous operation for 60 hours (Fig. 9c). Experimental and DFT calculation results had indicated that a lower nitrogen coordination number had endowed Co with more unoccupied 3d orbitals, enhancing the adsorption and activation of CO_2 intermediates and reducing charge transfer resistance, thereby improving catalytic activity. In contrast, Co–N_4 had exhibited weak CO_2 activation ability and extremely low catalytic activity due to its saturated coordination. In conclusion, Co-based SACs exhibit excellent CO_2-to-CO conversion capability by regulating the coordination environment to optimize the adsorption energy of intermediates. Pyridine-type Co–N_4 was suitable for large-scale and stable CO production; heteroatom doping can balance adsorption strength to achieve high activity and selectivity; and lower coordination numbers (*e.g.*, Co–N_2) can enhance CO_2 activation and improve kinetic efficiency. These strategies precisely match reaction requirements, providing a clear direction for the design of high-performance eCO_2RR catalysts.

4.4 Cu-based SACs

The valence shell electronic configuration of Cu had differed from those of Ni, Fe, and Co. Specifically, the 3d orbital of Cu had been fully filled, while its 4s orbital had contained only one electron. This unique structure had endowed Cu with two key advantages: (1) Cu exhibits a balanced adsorption capacity for key intermediates such as carboxyl groups (*COOH) and carbon monoxide (*CO), allowing CO to temporarily reside on active sites without excessive adsorption that would block the sites. This had provided a time window for the collision and coupling of intermediates such as CO with *CO and CO with *CHO.[97] (2) The flexibility of electron transfer to adapt to multi-step coupling reactions: the fully filled 3d orbital had made the electron transfer behavior of Cu atoms more flexible when

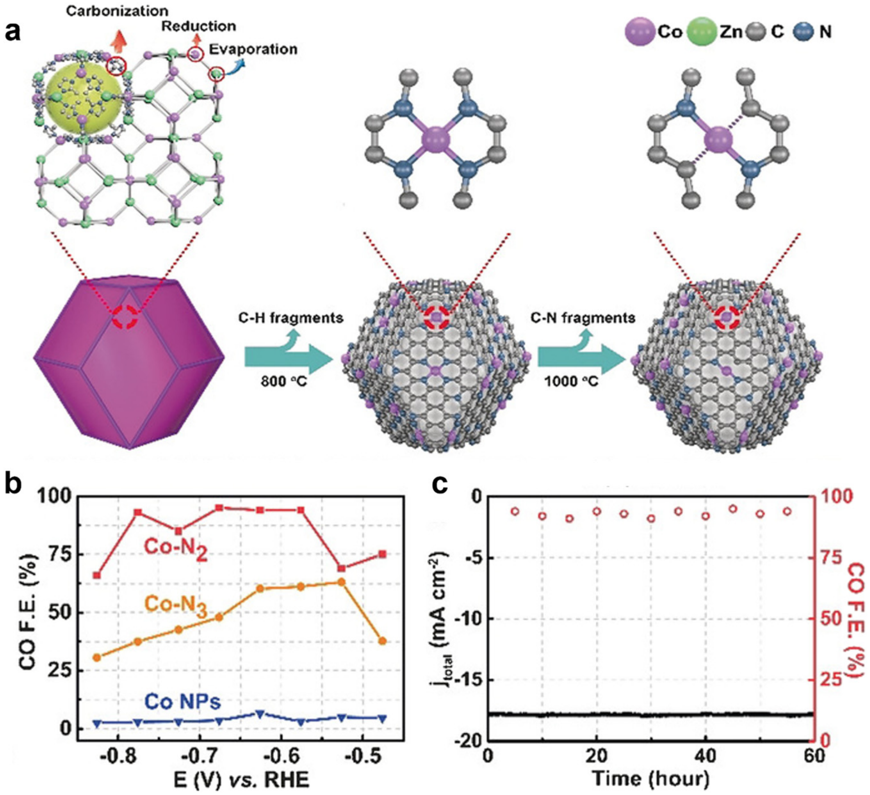

Fig. 9 (a) Formation mechanisms of Co–N_4 and Co–N_2; (b) FE_{CO} at varying applied potentials; (c) chronopotentiometric stability test at −0.63 V. Reprinted with permission from ref. 96. Copyright 2018, Wiley-VCH.

interacting with intermediates. Cu could not only transfer electrons to CO_2 molecules to activate them but also dynamically adjust electron gain and loss in multi-step reactions such as CO protonation, stabilize highly active intermediate species during coupling (*e.g.*, OC–CO, OC–CHO), and reduce the energy barrier for C–C bond formation.

Cheng *et al.*[98] had constructed three metal oxide-supported Cu single-atom catalysts (Al_2O_3–Cu_{SAC}, CeO_2–Cu_{SAC}, TiO_2–Cu_{SAC}) *via* ALD technology, and had thoroughly investigated the regulatory mechanism of metal–support interactions on the eCO_2RR performance. Studies had found that different supports had regulated the highest occupied molecular orbital (HOMO) of Cu sites through charge transfer, thereby dominating product selectivity: Al_2O_3–Cu_{SAC} had enhanced CO adsorption and weakened the C–O bond *via* electron back-donation, reducing the C–C coupling energy barrier and being more conducive to multi-carbon product formation; TiO_2–Cu_{SAC} had accelerated the activation and dissociation of water molecules, which had reduced the methane formation energy barrier but had also intensified the HER due to over-activated water molecules, affecting methane selectivity; CeO_2–Cu_{SAC} had not only promoted CO_2 activation but also inhibited C–C coupling through local electronic states, and the moderate degree of water molecule activation had facilitated the deep hydrogenation of *CO while suppressing the HER, exhibiting optimal methane selectivity. At a high current density of 400 mA cm^{-2}, the methane Faraday efficiency (FE_{CH_4}) had reached 70.3% with good stability for 70 hours. Additionally, the Al_2O_3-supported copper nanoparticle catalyst designed based on this mechanism had achieved a multi-carbon product Faraday efficiency of 81.3% at 900 mA cm^{-2}. Wu *et al.*[99] had proposed a self-healing copper single-atom catalyst design strategy for efficient electrocatalytic CO_2 methanation. Using PCN-222 as the precursor, a composite structure of ZrO_2 clusters and CuN_4 single atoms (ZrO_2/CuN_4) had been prepared *via* pyrolysis. After the HER pretreatment, partial cleavage of Cu–N bonds had been induced by *H attack, and the coordinatively unsaturated Cu atoms had spontaneously restructured with oxygen atoms on adjacent ZrO_2 clusters to form a CuN_1O_2 hybrid coordination structure (Fig. 10a). *In situ* Raman spectroscopy and XAFS had confirmed this dynamic restructuring process (Fig. 10b and c), and DFT calculations had indicated that this structure had optimized intermediate adsorption and electron distribution. Performance tests had shown that CuN_1O_2 had achieved a methane Faraday efficiency of 87.06 ± 3.22% at a current density of 500 mA cm^{-2} and had maintained 80.21 ± 1.01% at 1000 mA cm^{-2}, which were 3 times and 10 times higher than those of the original CuN_4, respectively. After 25 hours of continuous operation at 500 mA cm^{-2}, the activity decay had been less than 3%. Additionally, the CuN_1O_2 structure exhibits remarkable CH_4 selectivity over all carbon products in eCO_2RR, consistently surpassing 99% at current densities of −500 to −1000 mA cm^{-2} (Fig. 10d). The isolated nature of Cu active sites in traditional SACs often hinders the C–C coupling of *CO intermediates,

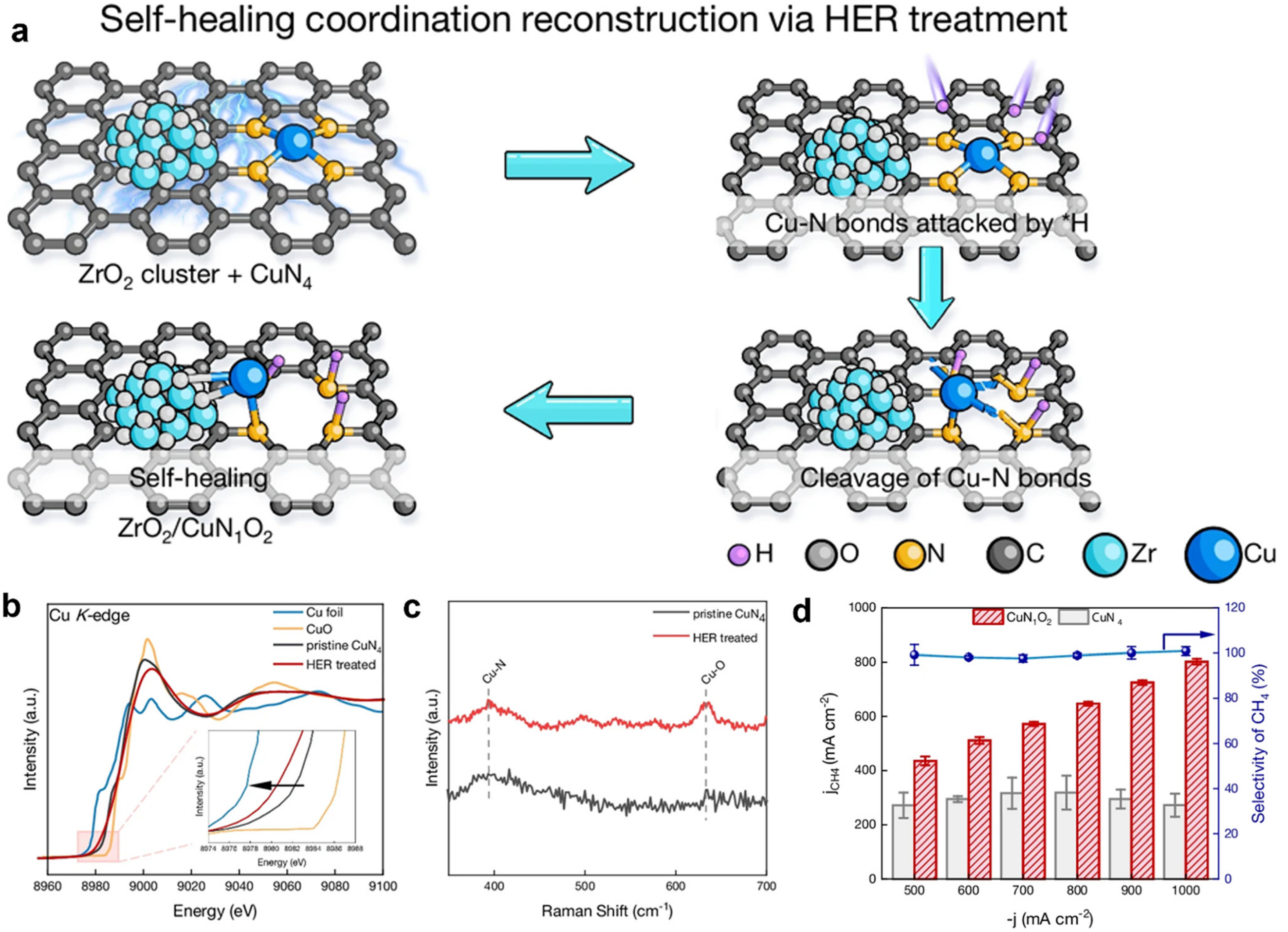

Fig. 10 (a) Schematic of structural reconstruction induced by hydrogen evolution treatment; (b) *in situ* Cu K-edge XANES spectra (the illustration shows an enlarged view of the energy range from 8977 to 8990 eV). and (c) the Raman spectra for ZrO_2/CuN_4 in pristine and after the HER treatment state; (d) CH_4 partial current densities of CuN_1O_2 and CuN_4 at different test currents, and CH_4 selectivity among carbon reduction products for CuN_1O_2. Reprinted with permission from ref. 98. Copyright 2025, Springer Nature.

making it difficult to efficiently produce C_2^+ products. However, this issue can be alleviated by designing the synergistic effect between metal centers and adjacent atoms. Zheng *et al.*[100] reported a Cu SAC synthesized *via* a temperature-tuned nitrogen coordination strategy. Their study revealed that the pyrolysis temperature can regulate the Cu doping concentration and the distance between adjacent Cu–N_x sites, thereby dominating the catalytic product selectivity: when the molar concentration of Cu reaches 4.9%, the distance between neighboring Cu–N_2 sites shortens, forming a synergistic effect to promote the C–C coupling of *CO intermediates. As a result, the Cu–N–C-800 catalyst achieves $FE_{C_2H_4}$ of 24.8% at −1.4 V; when the molar concentration of Cu was below 2.4%, the Cu–N_x sites were distributed in isolation, inhibiting C–C coupling and facilitating the deep hydrogenation of *CO. The Cu–N–C-900 catalyst exhibits a maximum FE_{CH_4} of 38.6% at −1.6 V and maintains stable operation for 10 hours. DFT calculations further confirm that adjacent Cu–N_2 sites tend to produce C_2H_4 due to the lower free energy for C–C coupling, while isolated Cu–N_2 and Cu–N_4 sites are more inclined to generate CH_4. In conclusion, the distribution pattern of active sites in Cu SACs dominates product selectivity: isolated single Cu sites, due to the lack of synergistic effects, tend to retain the adsorption and conversion of *CO intermediates in the CO formation pathway, while the efficient synthesis of C_2^+ products relies on multi-site synergism, which requires constructing a synergistic environment of adjacent active sites through regulatory strategies.

5 Summary and outlook

SACs had emerged as a crucial research direction in the eCO_2RR field, owing to their near-100% atomic utilization efficiency, well-defined active sites, and excellent selectivity. They had provided an efficient pathway for achieving carbon resource recycling and low-carbon energy conversion. What distinguishes this work is its integrated interpretation of mature synthesis strategies through the unique lens of a “dispersion–stabilization–performance” correlation. These techniques not only suppress metal agglomeration and construct stable anchoring sites *via* enhanced metal–support interactions but also precisely tailor the coordination environment of single atoms, laying a foundation for targeted performance optimization. Meanwhile, this work focuses on non-noble metal systems and systematically clarifies how their catalytic potential was unlocked through structural regulation: Ni-, Fe-, and Co-based single-atom catalysts achieve high CO selectivity by optimizing the adsorption–desorption energies of *COOH/*CO intermediates, while Cu-based single-atom catalysts, leveraging their unique electronic structures, exhibit irreplaceable advantages in the synthesis of multi-carbon products and methane. Beyond isolated discussions of synthesis or catalysis, this review emphasizes that the essence of single-atom catalyst performance optimization lies in the synergistic modulation of metal center selection, coordination environment regulation, and support electronic tuning. This integrated framework precisely matches the adsorption–desorption energies of key intermediates, reduces reaction energy barriers, and suppresses side reactions such as the HER.

Based on the aforementioned design principles, combined with current research bottlenecks and practical application requirements, the following specific research roadmap was proposed to provide a clear direction for the industrial advancement and performance breakthrough of SACs:

(1) Precise synthesis and large-scale preparation of high-loading and stable SACs: to address the issue that most single-atom catalysts (SACs) had exhibited low loadings (typically <5 wt%) and had been prone to deactivation under high current densities due to atomic agglomeration or active site poisoning, continuous innovations in synthesis strategies, novel supports, and coordination strategies had been required. These innovations aimed to fabricate SACs with high loadings while enhancing their anti-agglomeration and anti-poisoning capabilities, thereby meeting the requirements for industrial-scale long-term operation.

(2) Product-oriented rational design of single-atom to multi-atom catalysts: dual-atom and tri-atom catalysts excel in the eCO_2RR for C_2^+ products,[101] leveraging multi-metal synergy to regulate intermediate adsorption–desorption and electron transfer. Adjacent sites offer C/O-affinity centers to stabilize *COOH and *CO, breaking SACs' linear scaling limitation and lowering C–C coupling barriers. Homonuclear/heteronuclear electronic interactions optimize the d-band center, avoiding *CO over-adsorption poisoning or weak adsorption loss to favor pathways like *CO dimerization. Integrating *in situ*/operando characterization, machine learning, and DFT calculations reveals active site evolution and mechanisms, while precise design of multi-metal combinations and interatomic distances enhances selectivity, advancing efficient, low-cost C_2^+ production.

(3) Efficient screening and performance breakthrough of eCO_2RR catalysts: by integrating high-throughput experimental data, precise DFT calculation results, and machine learning (ML) algorithms, an integrated database covering catalyst structures, electronic properties, and catalytic performance can be constructed.[102,103] Through feature engineering, key descriptors such as active site types, coordination environment parameters, and intermediate adsorption energies were extracted to deeply explore the intrinsic structure–performance relationships, enabling the rational design and efficient screening of SACs. Meanwhile, combining the ability of deep learning to predict complex reaction pathways with the capture of dynamic catalytic processes by *in situ*/operando characterization techniques, the reaction mechanism of the eCO_2RR and the evolution law of active sites were accurately revealed, providing solid support for the development of SACs with high activity, excellent selectivity, and long-term stability.

(4) Adaptation for industrial-scale applications: most existing studies had been based on laboratory-scale H-type cells or small flow cells. Further optimization of the large-scale synthesis process of catalysts, development of electrode preparation technologies suitable for industrial electrolyzers, reduction of costs, and improvement of mass transfer efficiency had been necessary to promote the eCO_2RR technology from laboratory research to practical applications.

In the future, with the innovation of synthesis technologies, the clarification of structure–activity relationships, and the improvement of industrialization processes, SACs had been expected to achieve the unification of high activity, high selectivity, long-term stability, and low cost in the eCO_2RR field, providing core technical support for the achievement of global carbon neutrality goals.

Author contributions

Chao Xu: conceptualization, writing – original draft. Jinbing Wen: writing – review. Weikang Yuan: supervision. Xuezhi Duan: supervision and editing.

Conflicts of interest

The authors declare no conflict of interest.

Data availability

No primary research results, software or code have been included and no new data were generated or analysed as part of this review.

Acknowledgements

This work was financially supported by the National Key R&D Program of China (2022YFA1503804), the Science and Technology Commission of Shanghai Municipality Strategic Frontier Dedicated Project on Green Fuels (25DP30GF210), the Science and Technology Commission of Shanghai Municipality Key Technology R&D Plan program (25DZ3000100) and Key Basic Research Program (23JC1403300), the Guangxi Science and Technology Program (LT2504240025-3).

References

1 A. Wagner, C. D. Sahm and E. Reisner, Towards molecular understanding of local chemical environment effects in

electro- and photocatalytic CO_2 reduction, *Nat. Catal.*, 2020, **3**, 775–786.

2 Y. Zhang, H. Jiang, A. Kumar, H. Zhang, Z. Li, T. Xu, Y. Pan, Y. Wang, Z. Liu, G. Zhang and Z. Yan, Boosting the Ni–Zn interplay via O/N dual coordination for high-efficiency CO_2 electroreduction, *Carbon Energy*, 2023, **5**, e341.

3 Y. Wang, F. Ma, P. Zhang, G. Zhang, Z. Zhao, X. Zheng, H. Zhao, J. Zhang, Y. Dong and Y. Zhu, Tuning *CO–*CHO dimerization via twisted electron localization of asymmetrically coordinated Cu–Cu dual sites by P and N scatterings boosts CO_2 electroreduction, *ACS Catal.*, 2025, **15**, 17703–17714.

4 S. Chu and A. Majumdar, Opportunities and challenges for a sustainable energy future, *Nature*, 2012, **488**, 294–303.

5 X. Deng, D. Alfonso, T.-D. Nguyen-Phan and D. R. Kauffman, Breaking the limit of size-dependent CO_2RR selectivity in silver nanoparticle Electrocatalysts through electronic metal–carbon interactions, *ACS Catal.*, 2023, **13**, 15301–15309.

6 S. Liu, H. Tao, L. Zeng, Q. Liu, Z. Xu, Q. Liu and J.-L. Luo, Shape-dependent electrocatalytic reduction of CO_2 to CO on triangular silver nanoplates, *J. Am. Chem. Soc.*, 2017, **139**, 2160–2163.

7 A. Goyal, G. Marcandalli, V. A. Mints and M. T. M. Koper, Competition between CO_2 reduction and hydrogen evolution on a gold electrode under well-defined mass transport conditions, *J. Am. Chem. Soc.*, 2020, **142**, 4154–4161.

8 S. Wang, H. D. Jung, H. Choi, J. Kim, S. Back and J. Oh, Delicate control of a gold-copper oxide tandem structure enables the efficient production of high-value chemicals by electrochemical carbon dioxide reduction, *Nano Energy*, 2024, **130**, 110176.

9 W.-T. Chen, H. W. Shiu, Y.-X. Chen, E. Batsaikhan, Y.-L. Lai, S. L. Cheng, T. Araki, J.-F. Lee, M. Hayashi and Y.-J. Hsu, Highly selective toward HER or CO_2RR by regulating Cu single and dual atoms on g-C_3N_4, *Adv. Funct. Mater.*, 2025, e14183.

10 R.-Z. Xiong, H.-M. Xu, H.-R. Zhu, Z.-J. Zhang and G.-R. Li, Recent progress in Cu-based electrocatalysts for CO_2 reduction, *Chem. Eng. J.*, 2025, **505**, 159210.

11 G. Sun, R. Luo, D. Fu, K. Wu, X. Wang, X. Bian, Z. Lu, X. Chang, Z. Wang, S. Huang, Y. Zhu, J. Zhou, S. Chen, C. Pei, Z.-J. Zhao and J. Gong, Full utilization of noble metals by atom abstraction for propane dehydrogenation, *Science*, 2025, **390**, eadw3053.

12 L. Wu, T. Guo and T. Li, Data-driven high-throughput rational design of double-Aatom catalysts for oxygen evolution and reduction, *Adv. Funct. Mater.*, 2022, **32**, 2203439.

13 S. Liu, Y. Wang, K. F. Lyu, X. Lan and T. Wang, A one-pot strategy for anchoring single Pt atoms in MOFs with diverse coordination environments, *Nat. Synth.*, 2024, **3**, 1158–1167.

14 Y. Chen, S. Ji, C. Chen, Q. Peng, D. Wang and Y. Li, Single-atom catalysts: Synthetic strategies and electrochemical applications, *Joule*, 2018, **2**, 1242–1264.

15 Q. Zheng, H. Xu, Y. Yao, J. Dai, G. Zhan, J. Wang, B. Zhou, R. Wang, K. Wang, R. Zhao, B. Yang and L. Zhang, Regulation of Rh single-atom coordination for enhanced reverse hydrogen spillover and efficient electrochemical dechlorination, *J. Am. Chem. Soc.*, 2025, **147**, 44032–44040.

16 B. Peng, H. She, Z. Wei, Z. Sun, Z. Deng, Z. Sun and W. Chen, Sulfur-doping tunes p-d orbital coupling over asymmetric Zn-Sn dual-atom for boosting CO_2 electroreduction to formate, *Nat. Commun.*, 2025, **16**, 2217.

17 R. Lang, W. Xi, J.-C. Liu, Y.-T. Cui, T. Li, A. F. Lee, F. Chen, Y. Chen, L. Li, L. Li, J. Lin, S. Miao, X. Liu, A.-Q. Wang, X. Wang, J. Luo, B. Qiao, J. Li and T. Zhang, Non defect-stabilized thermally stable single-atom catalyst, *Nat. Commun.*, 2019, **10**, 234.

18 Y. Jiang, Z. Chen, T. Peng, L. Jiao, X. Pan, H.-L. Jiang and X. Bao, Single-atom Fe catalysts with improved metal loading for efficient ammonia synthesis under mild conditions, *Angew. Chem., Int. Ed.*, 2025, **64**, e202501190.

19 D. Yan, J. Chen and H. Jia, Temperature-induced structure reconstruction to prepare a thermally stable single-atom platinum catalyst, *Angew. Chem., Int. Ed.*, 2020, **59**, 13562–13567.

20 J. Jones, H. Xiong, A. T. DeLaRiva, E. J. Peterson, H. Pham, S. R. Challa, G. Qi, S. Oh, M. H. Wiebenga, X. I. Pereira Hernández, Y. Wang and A. K. Datye, Thermally stable single-atom platinum-on-ceria catalysts via atom trapping, *Science*, 2016, **353**, 150–154.

21 X. Yang, L. Xu and Y. Li, Do we achieve "1 + 1 > 2" in dual-atom or dual-single-atom catalysts?, *Coord. Chem. Rev.*, 2024, **516**, 215961.

22 N. Zhang, X. Zhang, L. Tao, P. Jiang, C. Ye, R. Lin, Z. Huang, A. Li, D. Pang, H. Yan, Y. Wang, P. Xu, S. An, Q. Zhang, L. Liu, S. Du, X. Han, D. Wang and Y. Li, Silver single-atom catalyst for efficient electrochemical CO_2 reduction synthesized from thermal transformation and surface reconstruction, *Angew. Chem., Int. Ed.*, 2021, **60**, 6170–6176.

23 Y. Li, C. Chen, R. Cao, Z. Pan, H. He and K. Zhou, Dual-atom Ag_2/graphene catalyst for efficient electroreduction of CO_2 to CO, *Appl. Catal., B*, 2020, **268**, 118747.

24 J. Li, Q. Guan, H. Wu, W. Liu, Y. Lin, Z. Sun, X. Ye, X. Zheng, H. Pan, J. Zhu, S. Chen, W. Zhang, S. Wei and J. Lu, Highly active and stable metal single-atom catalysts achieved by strong electronic metal–support interactions, *J. Am. Chem. Soc.*, 2019, **141**, 14515–14519.

25 Y. Wu, C. Chen, X. Yan, X. Sun, Q. Zhu, P. Li, Y. Li, S. Liu, J. Ma, Y. Huang and B. Han, Boosting CO_2 electroreduction over a cadmium single-atom catalyst by tuning of the axial coordination structure, *Angew. Chem., Int. Ed.*, 2021, **60**, 20803–20810.

26 H. Jin, S. Sultan, M. Ha, J. N. Tiwari, M. G. Kim and K. S. Kim, Simple and scalable mechanochemical synthesis of noble metal catalysts with single atoms toward highly efficient hydrogen evolution, *Adv. Funct. Mater.*, 2020, **30**, 2000531.

27 X. Cheng, S. Yin, J. Zhang, J. Yang, L. Chen, W. Wang, H. Liao, R. Huang, Y. Jiang, B. Zhang and S. Sun, Low-temperature pyrolysis: A universal route to high-loading single-atom catalysts for fuel cells, *Adv. Mater.*, 2025, **37**, 2501707.

28 L. Ran, Y. Xu, X. Zhu, S. Chen and X. Qiu, Mn single-atom tuning Fe-N-C catalyst enables highly efficient and durable oxygen electrocatalysis and zinc–air Batteries, *ACS Nano*, 2024, **18**, 750–760.

29 M. J. Hülsey, J. Zhang and N. Yan, Harnessing the wisdom in colloidal chemistry to make stable single-atom catalysts, *Adv. Mater.*, 2018, **30**, 1802304.

30 H. Yan, X. Zhao, N. Guo, Z. Lyu, Y. Du, S. Xi, R. Guo, C. Chen, Z. Chen, W. Liu, C. Yao, J. Li, S. J. Pennycook, W. Chen, C. Su, C. Zhang and J. Lu, Atomic engineering of high-density isolated Co atoms on graphene with proximal-atom controlled reaction selectivity, *Nat. Commun.*, 2018, **9**, 3197.

31 X. Liu, S. Jia, M. Yang, Y. Tang, Y. Wen, S. Chu, J. Wang, B. Shan and R. Chen, Activation of subnanometric Pt on Cu-modified CeO_2 via redox-coupled atomic layer deposition for CO oxidation, *Nat. Commun.*, 2020, **11**, 4240.

32 J. Fonseca and J. Lu, Single-atom catalysts designed and prepared by the atomic layer deposition technique, *ACS Catal.*, 2021, **11**, 7018–7059.

33 Y. Shi, Z.-R. Ma, Y.-Y. Xiao, Y.-C. Yin, W.-M. Huang, Z.-C. Huang, Y.-Z. Zheng, F.-Y. Mu, R. Huang, G.-Y. Shi, Y.-Y. Sun, X.-H. Xia and W. Chen, Electronic metal–support interaction modulates single-atom platinum catalysis for hydrogen evolution reaction, *Nat. Commun.*, 2021, **12**, 3021.

34 Q. Li, Q. Zhang, W. Xu, R. Zhao, M. Jiang, Y. Gao, W. Zhong, K. Chen, Y. Chen, X. Li and N. Yang, Sowing single atom seeds: A versatile strategy for hyper-low noble metal loading to boost hydrogen evolution reaction, *Adv. Energy Mater.*, 2023, **13**, 2203955.

35 Q. He, J. H. Lee, D. Liu, Y. Liu, Z. Lin, Z. Xie, S. Hwang, S. Kattel, L. Song and J. G. Chen, Accelerating CO_2 electroreduction to CO Over Pd single-atom catalyst, *Adv. Funct. Mater.*, 2020, **30**, 2000407.

36 G. Lu, S. Liu, Y.-F. Tang, M. Yu, Z.-Y. Wang, P.-F. Sui, X.-Z. Fu, Y. Sun, S. Liu and J.-L. Luo, The golden atomic ratio in binary nanoalloys for enhanced CO_2 electroreduction: Dual-metal synergy of AgPd, *ACS Catal.*, 2025, **15**, 17982–17990.

37 C. Guo, T. Zhang, X. Lu and C.-M. L. Wu, Rational design and effective control of gold-based bimetallic electrocatalyst for boosting CO_2 reduction reaction: A first-principles study, *ChemSusChem*, 2021, **14**, 2731–2739.

38 C. Hu, S. Bai, L. Gao, S. Liang, J. Yang, S.-D. Cheng, S.-B. Mi and J. Qiu, Porosity-induced high selectivity for CO_2 electroreduction to CO on Fe-doped ZIF-derived carbon catalysts, *ACS Catal.*, 2019, **9**, 11579–11588.

39 M. Qi, M. J. Zachman, Y. Li, Y. Zeng, S. Hwang, J. Liang, M. Lyons, Q. Zhao, Y. Mao, Y. Shao, Z. Feng, Z. Wang, Y. Zhao and G. Wu, Highly dense atomic Fe–Ni dual metal sites for efficient CO_2 to CO electrolyzers at industrial current densities, *Energy Environ. Sci.*, 2025, **18**, 5643–5656.

40 Y. Feng, Q. Mao, H. Yang, W. Zhou, D. Yang and Y. Gao, Ni single atom catalyst with high Ni–Nx content for efficient electrocatalytic reduction of CO_2, *Catal. Sci. Technol.*, 2025, **15**, 514–522.

41 C. Lu, K. Jiang, D. Tranca, N. Wang, H. Zhu, F. Rodríguez-Hernández, Z. Chen, C. Yang, F. Zhang, Y. Su, C. Ke, J. Zhang, Y. Han and X. Zhuang, Electrochemical reduction of carbon dioxide with nearly 100% carbon monoxide faradaic efficiency from vacancy-stabilized single-atom active sites, *J. Mater. Chem. A*, 2021, **9**, 24955–24962.

42 Y. Yang, W. Zhang, G. Wu, Q. Huang, J. Wen, D. Wang and M. Liu, Electronic structure tuning in Cu–Co dual single atom catalysts for enhanced COOH* spillover and electrocalytic CO_2 reduction activity, *Angew. Chem., Int. Ed.*, 2025, **64**, e202504423.

43 Z. Liang, L. Song, M. Sun, B. Huang and Y. Du, Atomically dispersed indium and cerium sites for selectively electroreduction of CO_2 to formate, *Nano Res.*, 2023, **16**, 8757–8764.

44 X. Zhang, R. Gao, Z. Zhang, D. Ren, H. Li, M. Feng and Z. Chen, Tailoring the coordination environment of single-atom catalysts for enhanced electrochemical CO_2-to-CO conversion efficiency, *Carbon Energy*, 2025, e70111.

45 R. Chen, J. Zhao, X. Zhang, Q. Zhao, Y. Li, Y. Cui, M. Zhong, J. Wang, X. Li, Y. Huang and B. Liu, Visualizing catalytic dynamics of single-cu-atom-modified SnS_2 in CO_2 electroreduction via rapid freeze-quench Mössbauer spectroscopy, *J. Am. Chem. Soc.*, 2024, **146**, 24368–24376.

46 B. Qiao, A. Wang, X. Yang, L. F. Allard, Z. Jiang, Y. Cui, J. Liu, J. Li and T. Zhang, Single-atom catalysis of CO oxidation using Pt_1/FeO_x, *Nat. Chem.*, 2011, **3**, 634–641.

47 F. Wang, K. Li, B. Li, C. Wang, Z. Li, Y. Zhang, W. Shan, Y. Yu, C. Zhang, Q. Fu, P. Ning, J. S. Francisco, X. C. Zeng and H. He, Identification of direct anchoring sites for monoatomic dispersion of precious metals (Pt, Pd, Ag) on CeO_2 support, *Angew. Chem., Int. Ed.*, 2024, **63**, e202318492.

48 L. Cao, F. Wei, Y. Chen, X. Pan, H. Cao, Y. Su, Y. Zhao, D. Chen, Y. Chai, L. Chen, J. Lin, S. Lin, X. Wang, X. Fu and T. Zhang, Atomic coordination editing achieves ultraproductive single-atom catalysts with ultralow loadings, *J. Am. Chem. Soc.*, 2025, **147**, 38752–38761.

49 Q. Wang, T. Luo, X. Cao, Y. Gong, Y. Liu, Y. Xiao, H. Li, F. Gröbmeyer, Y.-R. Lu, T.-S. Chan, C. Ma, K. Liu, J. Fu, S. Zhang, C. Liu, Z. Lin, L. Chai, E. Cortes and M. Liu, Lanthanide single-atom catalysts for efficient CO_2-to-CO electroreduction, *Nat. Commun.*, 2025, **16**, 2985.

50 Y. Ren, Y. Tang, L. Zhang, X. Liu, L. Li, S. Miao, D. Sheng Su, A. Wang, J. Li and T. Zhang, Unraveling the coordination structure-performance relationship in Pt_1/Fe_2O_3 single-atom catalyst, *Nat. Commun.*, 2019, **10**, 4500.

51 Z. Chen, C. Wang, X. Zhong, H. Lei, J. Li, Y. Ji, C. Liu, M. Ding, Y. Dai, X. Li, T. Zheng, Q. Jiang, H.-J. Peng and C. Xia, Achieving efficient CO_2 electrolysis to CO by local coordination manipulation of nickel single-atom catalysts, *Nano Lett.*, 2023, **23**, 7046–7053.

52 H. Xu, Z. Zhang, J. Liu, C.-L. Do-Thanh, H. Chen, S. Xu, Q. Lin, Y. Jiao, J. Wang, Y. Wang, Y. Chen and S. Dai, Entropy-stabilized single-atom Pd catalysts via high-entropy fluorite oxide supports, *Nat. Commun.*, 2020, **11**, 3908.

53 X. Guan, R. Han, H. Asakura, B. Wang, L. Chen, J. H. C. Yan, S. Guan, L. Keenan, S. Hayama, M. A. van Spronsen, G. Held, J. Zhang, H. Gu, Y. Ren, L. Zhang, Z. Yao, Y. Zhu, A. Regoutz, T. Tanaka, Y. Guo and F. R. Wang, Subsurface single-atom catalyst enabled by mechanochemical synthesis for oxidation chemistry, *Angew. Chem., Int. Ed.*, 2024, **63**, e202410457.

54 Y. Li, X. F. Lu, S. Xi, D. Luan, X. Wang and X. W. Lou, Synthesis of N-doped highly graphitic carbon urchin-like hollow structures loaded with single-Ni atoms towards efficient CO_2 electroreduction, *Angew. Chem., Int. Ed.*, 2022, **61**, e202201491.

55 Y. Ma, T. Xiao, K. Zhu, W. Zhang, Z. Yin, A. Dong, Z. Sun, D. Zhao and W. Li, Industry-level electrocatalytic CO_2 to CO enabled by 2D mesoporous Ni single atom catalysts, *Angew. Chem., Int. Ed.*, 2025, **64**, e202416629.

56 M. Wen, N. Sun, L. Jiao, S.-Q. Zang and H.-L. Jiang, Microwave-assisted rapid Synthesis of MOF-based single-atom Ni catalyst for CO_2 electroreduction at ampere-level current, *Angew. Chem., Int. Ed.*, 2024, **63**, e202318338.

57 J. Li, Y.-f. Jiang, Q. Wang, C.-Q. Xu, D. Wu, M. N. Banis, K. R. Adair, K. Doyle-Davis, D. M. Meira, Y. Z. Finfrock, W. Li, L. Zhang, T.-K. Sham, R. Li, N. Chen, M. Gu, J. Li and X. Sun, A general strategy for preparing pyrrolic-N_4 type single-atom catalysts via pre-located isolated atoms, *Nat. Commun.*, 2021, **12**, 6806.

58 K. Shen, M. Fan, Z. Liu, S. Satyanand, G. Yan, H.-L. Yu, M. Eisa, S. Caratzoulas, E. Stavitski, A. M. Karim, D. G. Vlachos, R. J. Gorte and J. M. Vohs, Single metal atom catalysts prepared by diluted atomic layer deposition, *ACS Appl. Mater. Interfaces*, 2025, **17**, 48279–48289.

59 F. Pan, B. Li, E. Sarnello, S. Hwang, Y. Gang, X. Feng, X. Xiang, N. M. Adli, T. Li, D. Su, G. Wu, G. Wang and Y. Li, Boosting CO_2 reduction on Fe-N-C with sulfur incorporation: Synergistic electronic and structural engineering, *Nano Energy*, 2020, **68**, 104384.

60 K. Li, S. Zhang, X. Zhang, S. Liu, H. Jiang, T. Jiang, C. Shen, Y. Yu and W. Chen, Atomic tuning of single-atom Fe–N–C catalysts with phosphorus for robust electrochemical CO_2 reduction, *Nano Lett.*, 2022, **22**, 1557–1565.

61 X. Wang, Y. Wang, L. Cui, W. Gao, X. Li, H. Liu, W. Zhou and J. Wang, Coordination-based synthesis of Fe single-atom anchored nitrogen-doped carbon nanofibrous membrane for CO_2 electroreduction with nearly 100% CO selectivity, *Chin. Chem. Lett.*, 2024, **35**, 110031.

62 J. He, L. Xu, C. Qin, J. Zhang, D. Liu, Q. Li, Z. Feng, J. Wang, P. Liu, H. Li and Z. Yang, Electron reservoir effect of adjacent Fe nanoclusters boosts atomic Fe active sites on porous carbon for the both electrocatalytic oxygen reduction and CO_2 reduction reaction, *Small*, 2024, **20**, 2405157.

63 J. Tuo, Y. Zhu, H. Jiang, J. Shen and C. Li, The effect of the coordination environment of atomically dispersed Fe and N Co-doped carbon nanosheets on CO_2 electroreduction, *ChemElectroChem*, 2020, **7**, 4767–4772.

64 L. Shen, L. Wang, Y. Ye, Z. Li and Q. Dai, Creation of intrinsic defects on ZIF-8 particles to facilitate electrochemical reduction of CO_2 over Fe single-atom catalyst, *Chem. Eng. J.*, 2024, **495**, 153073.

65 P. Zhang, J. Miao, B. Zhang, T. Gan, Y. Song, G. Li, J. Jiang, C. Xu and X. Sun, Tailoring short- and long-range electron transfer of single iron sites for boosted CO_2 electroreduction reaction at low overpotentials, *Chem. Eng. Sci.*, 2026, **320**, 122448.

66 L. Shen, L. Wang, Z. Li, Y. Ye and Q. Dai, Modification of single atomic Fe–N_4 catalytic site with sulfur to promote CO_2 electroreduction, *Carbon*, 2025, **242**, 120388.

67 S. Chen, X. Li, C.-W. Kao, T. Luo, K. Chen, J. Fu, C. Ma, H. Li, M. Li, T.-S. Chan and M. Liu, Unveiling the proton-feeding effect in sulfur-doped Fe–N–C single-atom catalyst for enhanced CO_2 electroreduction, *Angew. Chem., Int. Ed.*, 2022, **61**, e202206233.

68 Z. Jin, D. Jiao, Y. Dong, L. Liu, J. Fan, M. Gong, X. Ma, Y. Wang, W. Zhang, L. Zhang, Z. Gen Yu, D. Voiry, W. Zheng and X. Cui, Boosting electrocatalytic carbon dioxide reduction via self-relaxation of asymmetric coordination in Fe-based single atom catalyst, *Angew. Chem., Int. Ed.*, 2024, **63**, e202318246.

69 Y.-N. Gong, L. Jiao, Y. Qian, C.-Y. Pan, L. Zheng, X. Cai, B. Liu, S.-H. Yu and H.-L. Jiang, Regulating the coordination environment of MOF-templated single-atom nickel electrocatalysts for boosting CO_2 reduction, *Angew. Chem., Int. Ed.*, 2020, **59**, 2705–2709.

70 G. Hwa Jeong, Y. Chuan Tan, J. Tae Song, G.-Y. Lee, H. Jin Lee, J. Lim, H. Young Jeong, S. Won, J. Oh and S. Ouk Kim, Synthetic multiscale design of nanostructured Ni single atom catalyst for superior CO_2 electroreduction, *Chem. Eng. J.*, 2021, **426**, 131063.

71 W. Ren, X. Tan, C. Jia, A. Krammer, Q. Sun, J. Qu, S. C. Smith, A. Schueler, X. Hu and C. Zhao, Electronic regulation of nickel singleatoms by confined nickel nanoparticles for energy-efficient CO_2 electroreduction, *Angew. Chem., Int. Ed.*, 2022, **61**, e202203335.

72 M. Huang, B. Deng, X. Zhao, Z. Zhang, F. Li, K. Li, Z. Cui, L. Kong, J. Lu, F. Dong, L. Zhang and P. Chen, Template-sacrificing synthesis of well-defined asymmetrically coordinated single-atom catalysts for highly efficient CO_2 electrocatalytic reduction, *ACS Nano*, 2022, **16**, 2110–2119.

73 J. W. Lim, D. H. Choo, J. H. Cho, J. Kim, W. S. Cho, O. F. Ngome Okello, K. Kim, S. Lee, J. Son, S.-Y. Choi, J. K. Kim, H. W. Jang, S. Y. Kim and J.-L. Lee, A MOF-derived pyrrolic N-stabilized Ni single atom catalyst for selective electrochemical reduction of CO_2 to CO at high current density, *J. Mater. Chem. A*, 2024, **12**, 11090–11100.

74 B. Dai, M. Wang, H. Xu, H. Zheng, Y. Zhang, C. Ma, J. Wang, W. Qiao and L. Ling, Atomic-level engineering Ni-N_2O_2 interfacial structure for enhanced CO_2 electrocatalytic reduction efficiency, *J. Colloid Interface Sci.*, 2025, **690**, 137260.

75 Y. Chen, X. Pan, L. Li, M. Chen, H. Cao, Y. Zhao, X. Wang and J. Lin, Modulating electronic density of single-atom Ni center by heteroatoms for efficient CO_2 electroreduction, *Small*, 2025, **21**, 2411249.

76 W. Zhang, A. Mehmood, G. Ali, H. Liu, L. Chai, J. Wu and M. Liu, Nickel nanocluster-stabilized unsaturated Ni–N_3 atomic sites for efficient CO_2-to-CO electrolysis at industrial-level current, *Angew. Chem., Int. Ed.*, 2025, **64**, e202424552.

77 F. Zhang, J. Li, S. Chen, J. Li, R. Zhang, Y. Zhao, W.-Y. Zan and Y. Li, Highly stable and electron-rich Ni single atom catalyst for directed electroreduction of CO_2 to CO, *J. Catal.*, 2024, **440**, 115815.

78 W. Sun, S. Liu, H. Sun, H. Hu, J. Li, L. Wei, Z. Tian, Q. Chen, J. Su and L. Chen, Low-coordinated Ni single atom catalyst with carbon coordination for efficient CO_2 electroreduction, *Adv. Energy Mater.*, 2025, **15**, 2500283.

79 X. Su, B. Hu, Y. Zhang, C. Liu, C. Wang, L. Zheng, D. Zhao, J. Zhang and C. Chen, Built-in axial electric field-driven electron-rich monomolecular Co sites for promoting CO_2 electroreduction to CO over ultrawide potential window, *Angew. Chem., Int. Ed.*, 2025, **64**, e202511671.

80 H. Cheng, Z. Fan, X. Wu, M. Feng, W. Zheng, G. Lei, X. Li, F. Cui and G. He, Coordination engineering of the hybrid Co-C and Co-N active sites for efficient catalyzing CO_2 electroreduction, *J. Catal.*, 2022, **405**, 634–640.

81 Y.-T. Cheng, J.-Z. Peng, G.-T. Lai, X. Yue, F.-Z. Li, Q. Wang, L.-N. Chen and J. Gu, Edge-site Co–N_x model single-atom catalysts for CO_2 electroreduction, *ACS Catal.*, 2024, **14**, 8446–8455.

82 Y. Zhong, X. Kong, Z. Geng, J. Zeng, X. Luo and L. Zhang, Molecular modification of single cobalt sites boosts the catalytic activity of CO_2 electroreduction into CO, *ChemPhysChem*, 2020, **21**, 2051–2055.

83 Y. Pan, R. Lin, Y. Chen, S. Liu, W. Zhu, X. Cao, W. Chen, K. Wu, W.-C. Cheong, Y. Wang, L. Zheng, J. Luo, Y. Lin, Y. Liu, C. Liu, J. Li, Q. Lu, X. Chen, D. Wang, Q. Peng, C. Chen and Y. Li, Design of single-atom Co–N_5 catalytic site: A robust electrocatalyst for CO_2 reduction with nearly 100% CO selectivity and remarkable stability, *J. Am. Chem. Soc.*, 2018, **140**, 4218–4221.

84 J. Feng, H. Gao, L. Zheng, Z. Chen, S. Zeng, C. Jiang, H. Dong, L. Liu, S. Zhang and X. Zhang, A Mn-N_3 single-atom catalyst embedded in graphitic carbon nitride for efficient CO_2 electroreduction, *Nat. Commun.*, 2020, **11**, 4341.

85 X. Su, Z. Jiang, J. Zhou, H. Liu, D. Zhou, H. Shang, X. Ni, Z. Peng, F. Yang, W. Chen, Z. Qi, D. Wang and Y. Wang, Complementary operando spectroscopy identification of in-situ generated metastable charge-asymmetry Cu_2-CuN_3 clusters for CO_2 reduction to ethanol, *Nat. Commun.*, 2022, **13**, 1322.

86 L. Jiao, C. Mao, F. Xu, X. Cheng, P. Cui, X. Wang, L. Yang, Q. Wu and Z. Hu, Constructing gold single-atom catalysts on hierarchical nitrogen-doped carbon nanocages for carbon dioxide electroreduction to syngas, *Small*, 2024, **20**, 2305513.

87 R. Sui, J. Pei, J. Fang, X. Zhang, Y. Zhang, F. Wei, W. Chen, Z. Hu, S. Hu, W. Zhu and Z. Zhuang, Engineering Ag–N_x single-atom sites on porous concave N-doped carbon for boosting CO_2 electroreduction, *ACS Appl. Mater. Interfaces*, 2021, **13**, 17736–17744.

88 Y. Cui, C. Ren, Q. Li, C. Ling and J. Wang, Hybridization state transition under working conditions: Activity origin of single-atom catalysts, *J. Am. Chem. Soc.*, 2024, **146**, 15640–15647.

89 Y. Wang, P. Zhu, R. Wang, K. C. Matthews, M. Xie, M. Wang, C. Qiu, Y. Liu, H. Zhou, J. H. Warner, Y. Liu, H. Wang and G. Yu, Fluorine-tuned carbon-based nickel single-atom catalysts for scalable and highly efficient CO_2 electrocatalytic reduction, *ACS Nano*, 2024, **18**, 26751–26758.

90 J. Wang, K. Zhang, T. T. T. Nga, Y. Wang, Y. Shi, D. Wei, C.-L. Dong and S. Shen, Chalcogen heteroatoms doped nickel-nitrogen-carbon single-atom catalysts with asymmetric coordination for efficient electrochemical CO_2 reduction, *Chin. J. Catal.*, 2024, **64**, 54–65.

91 Y.-Z. Qiu, X.-M. Liu, W. Li, J. Li and H. Xiao, Transient dangling active sites of Fe(III)–N–C single-atom catalyst for efficient electrochemical CO_2 reduction reaction, *Angew. Chem., Int. Ed.*, 2025, **64**, e202424150.

92 Y. Zeng, J. Zhao, S. Wang, W. Wang, Y.-R. Lu, S. Xi, W. Xu, Y. Yoda, R. Masuda, X. Li, Y. Huang, B. Liu and T. Zhang, Unraveling the dynamic low-spin state evolution of single-Fe-atom sites for efficient CO_2 electroreduction, *J. Am. Chem. Soc.*, 2025, **147**, 42539–42548.

93 Q.-H. Guo, G.-L. Zhang, Y. Wu, X. Liang, L. Li and J.-J. Yang, Theoretical study on the electrocatalytic CO_2 reduction mechanism of single-atom Co complexed carbon-based (Co–Nχ@C) catalysts supported on carbon nanotubes, *ACS Appl. Mater. Interfaces*, 2024, **16**, 46270–46279.

94 Z. Zeng, J. Xu, Y. Zhao, J. Li, C. Du, Y. Sun and H. Xiong, Tuning the microenvironment of Co–N_4 ensemble for Co single-atom catalysts for electrocatalytic CO_2 reduction, *ChemCatChem*, 2024, **16**, e202400091.

95 J. Pei, H. Shang, J. Mao, Z. Chen, R. Sui, X. Zhang, D. Zhou, Y. Wang, F. Zhang, W. Zhu, T. Wang, W. Chen and Z. Zhuang, A replacement strategy for regulating local environment of single-atom Co-S_xN_{4-x} catalysts to facilitate CO_2 electroreduction, *Nat. Commun.*, 2024, **15**, 416.

96 X. Wang, Z. Chen, X. Zhao, T. Yao, W. Chen, R. You, C. Zhao, G. Wu, J. Wang, W. Huang, J. Yang, X. Hong, S. Wei, Y. Wu and Y. Li, Regulation of coordination number over single Co sites: Triggering the efficient electroreduction of CO_2, *Angew. Chem., Int. Ed.*, 2018, **57**, 1944–1948.

97 J. Satra, S. Goswami, S. J. Phukan, C. Bhaumik, S. Ghanta, B. Pakhira, S. Garai, M. Roy and T. K. Misra, Contemporary progress on single-atom electrocatalysts for H_2 evolution and CO_2 reduction reaction: Insights, bottlenecks, and perspectives, *Chem. – Asian J.*, 2025, **20**, e00841.

98 Y. Zhang, F. Chen, X. Yang, Y. Guo, X. Zhang, H. Dong, W. Wang, F. Lu, Z. Lu, H. Liu, H. Liu, Y. Xiao and Y. Cheng, Electronic metal-support interaction modulates Cu electronic structures for CO_2 electroreduction to desired products, *Nat. Commun.*, 2025, **16**, 1956.

99 W. Shen, X. Gao, Q. Liu, P. Li, R. Huang, Y. Tan, Z. Wang, Y. Zhang, F. Zhao, X. Wang, S. Ji, X. Zheng, Y. Zhang and Y. Wu, Self-healing Cu single-atom catalyst for high-performance electrocatalytic CO_2 methanation, *Nat. Commun.*, 2025, **16**, 7943.

100 A. Guan, Z. Chen, Y. Quan, C. Peng, Z. Wang, T.-K. Sham, C. Yang, Y. Ji, L. Qian, X. Xu and G. Zheng, Boosting CO_2 electroreduction to CH_4 via tuning neighboring single-copper sites, *ACS Energy Lett.*, 2020, **5**, 1044–1053.

101 J. Yang, X. Liu, Z. Li, S. Xi, J. Sun, H. Yuan, W. Liu, T. Wang, Y. Gao, H. Wang, J. Wang, J. S. Chen, R. Wu, Y.-W. Zhang and J. Wang, Quasi-copper-mers enable high-performance catalysis for CO_2 reduction, *Adv. Sci.*, 2023, **10**, 2303297.

102 Y. Shi and Z. Liang, Machine learning accelerates the screening of single-atom catalysts towards CO_2 electroreduction, *Appl. Catal., A*, 2024, **676**, 119674.

103 X. Wen, X. Geng, G. Su, Y. Li, Q. Li, Y. Yi and L. Liu, Machine learning-driven design of single-atom catalysts for carbon dioxide valorization to high-value chemicals: A review of photocatalysis, electrocatalysis, and thermocatalysis, *Green Chem.*, 2025, **27**, 4898–4925.